Available online at www.sciencedirect.com
ScienceDirect
Comput. Methods Appl. Mech. Engrg. 403 (2023) 115763
Computer methods in applied mechanics and engineering
www.elsevier.com/locate/cma

A C^0-nonconforming virtual element methods for the vibration and buckling problems of thin plates

Dibyendu Adak[a,b,*], David Mora[a,c], Iván Velásquez[d]

[a] GIMNAP, Departamento de Matemática, Universidad del Bío-Bío, Concepción, Chile
[b] Department of Mechanical Engineering, Indian Institute of Technology Madras, Chennai 600036, India
[c] CI^{2}MA, Universidad de Concepción, Concepción, Chile
[d] Departamento de Ciencias Básicas, Universidad del Sinú Elías Bechara Zainum, Montería, Colombia

Received 3 August 2022; received in revised form 1 November 2022; accepted 2 November 2022
Available online xxxx

Abstract

In this work, we study the C^0-nonconforming VEM for the fourth-order eigenvalue problems modeling the vibration and buckling problems of thin plates with clamped boundary conditions on general shaped polygonal domain, possibly even nonconvex domain. By employing the *enriching* operator, we have derived the convergence analysis in discrete H^2 seminorm, and H^1, L^2 norms for both problems. We use the Babuška–Osborn spectral theory (Babuška and Osborn, 1991), to show that the introduced schemes provide well approximation of the spectrum and prove optimal order of rate of convergence for eigenfunctions and double order of rate of convergence for eigenvalues. Finally, numerical results are presented to show the good performance of the method on different polygonal meshes.

Keywords: Nonconforming, Virtual element method, Vibration, Buckling, Spectral problems, Error estimates

1. Introduction

The numerical approximations of eigenvalue problems such as vibrations and buckling problems are important research topic in numerical analysis since the model problems are frequently encountered in engineering applications such as bridge, ship, and aircraft design. In view of application, we are dedicated to developed efficient numerical schemes and convergence analysis of the following model problems. The vibration eigenvalue problem **(VEP)** can be reads as follows. Find $(\lambda, u) \in \mathbb{R} \times H_0^2(\Omega)$ with $u \neq 0$ such that

$$\Delta^2 u = \lambda u \quad \text{in} \quad \Omega, \tag{1.1a}$$

$$u = \partial_{\boldsymbol{n}} u = 0 \quad \text{on} \quad \Gamma, \tag{1.1b}$$

where $\lambda = \omega^2$, with $\omega > 0$ being the vibration frequency, and $\partial_{\boldsymbol{n}}$ denotes the normal derivative. To simplify the notation we have taken the Young modulus and the density of the plate, both equal to 1. On the other hand, we

* Corresponding author at: GIMNAP, Departamento de Matemática, Universidad del Bío-Bío, Concepción, Chile.
E-mail addresses: dadak@ubiobio.cl (D. Adak), dmora@ubiobio.cl (D. Mora), ivanvelasquez@unisinu.edu.co (I. Velásquez).

https://doi.org/10.1016/j.cma.2022.115763
0045-7825/

have the buckling eigenvalue problem **(BEP)**, which can be stated as follows. Find $(\lambda, u) \in \mathbb{R} \times H_0^2(\Omega)$ with $u \neq 0$ such that

$$\Delta^2 u = -\lambda \Delta u \qquad \text{in} \qquad \Omega, \tag{1.2a}$$

$$u = \partial_{\boldsymbol{n}} u = 0 \qquad \text{on} \qquad \Gamma. \tag{1.2b}$$

There are various numerical schemes study and understand the approximated solutions of the buckling and vibration problems, e.g., FEMs [1–4], C^1-VEM [5–8] and the references therein. We emphasize that the computational cost for C^1-FEM is high, and it decreases significantly in case of VEM approximation. In addition to this advantage, we focus on developing a nonconforming VEM scheme for the above model problems on general type of domains (even nonconvex).

The Virtual element method (VEM) is a numerical technique to compute solutions of partial differential equations arising in mathematical models from science and engineering on finite dimensional space. This new technology possesses many noticeable features such as a solid mathematical background, a combined formulation for elements irrespective of geometric shapes, including nonconvex and oddly shaped elements, an easy extension to higher dimensions, arbitrary orders of accuracy and regularity, and a simpler mesh discretizations for moving boundary domains and interface problems. These features attract researchers from both engineering and mathematical communities and have been studied to approximate different model problems, e.g., elliptic equations [9–12], convection-dominated diffusion–reaction equations [13,14], nonlocal plate problems [15], just to mention a few applications. The nonconforming VEM, originally proposed in [16] for elliptic problems, was later extended to Stokes equations [17,18], eigenvalue problems [19], plate bending problems [20,21], biharmonic equations [22–24] and, then, generalized to polyharmonic problems in any number of spatial dimensions [25]. Conforming VEM are studied extensively for different second and fourth order eigenvalue problems [5–8,26–30]. Also, nonconforming VEM for second order eigenvalue problem has been presented in [19]. However, to the best of our knowledge nonconforming VEM for fourth order eigenvalue problems has not been studied.

In this article, we have developed, for the first time, an unified analysis of C^0-nonconforming VEM for **VEP** and **BEP** on general type of domains. We have investigated the continuous formulations associated with (1.1) and (1.2) through certain continuous, compact and self-adjoint operators. Based on the transverse displacement of the midplane of a thin plate, we define and analyze discrete solution operators on finite dimensional discrete space to examine the characteristic of spectrum of discrete formulation associated with both eigenproblems. Further, the authors in [21] introduced C^0-nonconforming VEM to approximate plate bending problems in a convex domain, where the exact solutions have more regularity. Such analysis cannot be adopted to derive convergence analysis of **VEP** and **BEP** when the associated eigenfunctions have less regularity, particularly on the nonconvex domain. Remembering this difficulty, we bypass the problem by adopting *Enriching* operator defining from nonconforming VEM to its C^1 continuous counter space. Finally, we have derived the convergence analysis in L^2, and H^1 norms and broken H^2 semi-norm, and asserted the convergence of the eigenfunctions, and eigenvalues by exploiting *Babuška–Osborn* theory [31]. An immediate practical application of this work is to study the spectrum of the biharmonic operators modeling bridges, e.g. [32, Equation 7]. Based on the previous observations, we summarize our contributions to the development of nonconforming VEM for the approximation of the eigenproblems as follows:

- C^0-nonconforming VEM schemes are proposed to compute eigenvalues of **VEP**, **BEP** with the assumption of less regular analytically solutions and a priori error estimates are derived in a unified way.
- The framework of convergence analysis is robust, which means we have shown the convergence of the associated source problems in the norms of their respective continuous spaces.
- We have offered various types of numerical experiments to cover practical examples including plates with various boundary conditions, usually encountered in engineering applications.

The article is organized as follow. In Section 2, we present the variational formulations associated with model problems (1.1), and (1.2) in a unified way. Further, we have defined the source problems, and solution operator allied with weak continuous formulations Problem 1. In Section 3, we have introduced lowest order C^0-nonconforming VEM space and designed discrete schemes to approximate model problems. By introducing *enriching* operator, *a priori* error estimates are derived in H^2 seminorm, and H^1, L^2 norms for source problems in Section 4 which is followed by convergence analysis of spectrum of solution operators and consequently spectrum of the model problems. Finally, we investigate behavior of our proposed schemes through numerical experiments and confirm the theoretical expectation in Section 6. In Section 7, we postulate our global remark and possible future developments of our work.

2. Preliminaries and weak formulations of the problems

2.1. Notations

Throughout this paper, we follow the convention of Sobolev spaces of Ref. [33]. Accordingly, we denote the space of square integrable functions defined on any open, bounded, connected domain $\omega \subset \mathbb{R}^2$ with boundary $\partial\omega$ by $L^2(\omega)$, and the Hilbert space of functions in $L^2(\omega)$ with all partial derivatives up to a positive integer m also in $L^2(\omega)$ by $H^m(\omega)$, cf. [33]. We endow $H^m(\omega)$ with a norm and a seminorm that we denote as $\|\cdot\|_{m,\omega}$ and $|\cdot|_{m,\omega}$, respectively. We denote the space of polynomials of degree up to a given integer $l \geq 0$ and defined on ω by $\mathbb{P}_l(\omega)$, and, for $l = -1$, we conventionally assume that $\mathbb{P}_{-1} = \{0\}$. We denote the unit vector that is orthogonal to $\partial\omega$ and pointing out of ω by $\mathbf{n}_\omega = (n_1, n_2)^T$, and the unit vector that is tangent to $\partial\omega$ by $\mathbf{t}_\omega = (t_1, t_2)^T$ and oriented such that $t_1 = -n_2$ and $t_2 = n_1$. To avoid ambiguity, we express $\partial_{\mathbf{n}}\phi = \mathbf{n} \cdot \nabla\phi$ and $\partial_t\phi = \boldsymbol{t} \cdot \nabla\phi$ to denote the normal and tangential derivatives along an edge with unit normal and tangential vectors $\mathbf{n}$ and $\boldsymbol{t}$, respectively. The *Hessian matrix of* ϕ, defined as $\mathcal{H}\phi := (\partial_{ij}\phi)_{1\leq i,j\leq 2}$; The *gradient of* u, defined as the vector $\nabla u = (\partial_j u)_{j,=1,2}$; We denote the inner-product of any pair of tensors $\boldsymbol{\tau} = (\tau_{ij})_{i,j=1,2}$ and $\boldsymbol{\sigma} = (\sigma_{ij})_{i,j=1,2}$ by $\boldsymbol{\tau} : \boldsymbol{\sigma} = \sum_{i,j=1}^2 \tau_{ij}\sigma_{ij}$. With the previous notation, we signify the L^2-inner products of scalar and tensor functions as

$$\mathcal{B}^0(\phi, \psi) = \int_\omega \phi\,\psi, \quad \mathcal{B}^\nabla(\phi, \psi) = \int_\omega \nabla\phi \cdot \nabla\psi, \quad \mathcal{A}^{\mathcal{D}}(\phi, \psi) = \int_\omega \mathcal{H}\phi : \mathcal{H}\psi. \tag{2.1}$$

Further, we omit the subscript ω on the left of (2.1) if $\omega = \Omega$. Finally, we bring forth that the letter C, possibly with a subindex, a superindex, or a modifier on top such as "$\widetilde{C}$" or "$\widehat{C}$", or "C_Ω" denote a positive constant whose value can be different at any instance and that is independent of h but may depend on the other parameters of the problem and the discretization that we will introduce in the next sections.

Remark 2.1. The spectral problems (1.1) and (1.2) can be analyzed with mixed boundary conditions. For instance, if the plate is considered to be clamped on part Γ_C, simply supported (S.S.) on part Γ_S and free on Γ_F:

$$\Gamma := \Gamma_C \cup \Gamma_S \cup \Gamma_F.$$

We assume that Γ_C, Γ_S and Γ_F are finite sums of connected components and that Γ_C, Γ_S are given such that rigid-body motions are avoided. Thus, in this case, the deflection of the plate, belongs to the Sobolev space:

$$V := \{v \in H^2(\Omega) : v = 0 \text{ on } \Gamma_C \cup \Gamma_S, \ \ \partial_{\mathbf{n}}v = 0 \text{ on } \Gamma_C\}.$$

In this case, the theoretical and numerical analysis presented in the next sections can be developed with the same arguments as those applied for a clamped plate. We mention that numerical verification of test cases involving other types of boundary conditions will be addressed in Section 6, where we observe optimal convergence.

2.2. The continuous spectral variational formulations

Now, we present the variational formulations associated to the spectral problems **(VEP)** and **(BEP)** (cf. (1.1) and (1.2), respectively). We denote $\mathcal{V} := \{v \in H^2(\Omega) : v = \partial_{\mathbf{n}}v = 0 \text{ on } \partial\Omega\}$. With this end, we multiply Eq. (1.1a) by $v \in \mathcal{V}$ (respectively, (1.1b)), integrate by parts twice, and apply the boundary conditions (1.1b) (respectively, (1.2b)) to obtain the following spectral variational formulations:

Problem 1. Find $(\lambda^\dagger, u^\dagger) \in \mathbb{R} \times \mathcal{V}$, with $u \neq 0$ such that

$$\mathcal{A}^{\mathcal{D}}(u, v) = \lambda\mathcal{B}^\dagger(u, v) \qquad \forall v \in \mathcal{V},$$

where we have defined the bilinear forms in (2.1). In Problem 1, we use the superscript $\dagger \in \{0, \nabla\}$ ($\dagger = 0$ or $\dagger = \nabla$) to refer a generic definition, property or result that is valid for both the eigenvalue problems analyzed in this work and will follow the same symbol of variables in the forthcoming part of the article. By exploiting standard theory on Sobolev spaces, we summarize the following results.

Lemma 2.1. *There exist positive constants* C_Ω *and* $\widehat{C}$ *such that*

$$|\mathcal{A}^{\mathcal{D}}(u, v)| \leq C_\Omega |u|_{2,\Omega}|v|_{2,\Omega} \ \forall u, v \in H^2(\Omega), \quad |\mathcal{B}^0(u, v)| \leq C_\Omega \|u\|_{0,\Omega}\|v\|_{0,\Omega} \ \forall u, v \in L^2(\Omega),$$
$$|\mathcal{B}^\nabla(u, v)| \leq C_\Omega |u|_{1,\Omega}|v|_{1,\Omega} \ \forall u, v \in H^1(\Omega), \quad \mathcal{A}^{\mathcal{D}}(v, v) \geq \widehat{C}|v|_{2,\Omega}^2 \qquad \forall v \in \mathcal{V}.$$

The ellipticity condition of $\mathcal{A}^{\mathcal{D}}(\cdot,\cdot)$ follows from the fact that $\|\mathcal{H}v\|_{0,\Omega}$ is a norm on $\mathcal{V}$ which it is equivalent to the usual one.

2.3. The analysis of the source problems

To avoid annoying repetition, we consider the following auxiliary notations, $H^0 \equiv L^2(\Omega)$ and $H^\nabla \equiv H^1(\Omega)$. Now, we introduce the following solution operators associated to the vibration and buckling problems of thin plates (cf. Problem 1).

$$\begin{aligned} &\mathcal{S}^\dagger : H^\dagger \to H^\dagger \\ &f^\dagger \longmapsto \mathcal{S}^\dagger f^\dagger =: \widetilde{u}^\dagger, \end{aligned} \tag{2.2}$$

where $\widetilde{u}^\dagger$ is the unique solution of the following source problem

$$\mathcal{A}^{\mathcal{D}}(\widetilde{u}^\dagger, v) = \mathcal{B}^\dagger(f^\dagger, v) \qquad \forall v \in \mathcal{V}. \tag{2.3}$$

We have that the linear operators $\mathcal{S}^\dagger$ are well defined and bounded. Notice that $(\lambda, u^\dagger) \in \mathbb{R}\times\mathcal{V}$ solves problem (2.3) if and only if $\mathcal{S}^\dagger u^\dagger = \mu u^\dagger$ with $\mu \neq 0$ and $u^\dagger \neq 0$, in which case $\mu := \frac{1}{\lambda}$. In addition, we also have that $\mathcal{S}^\dagger$ is self-adjoint with respect to the inner-product $\mathcal{B}^\dagger(\cdot,\cdot)$. Indeed, given $f, g \in H^\dagger$,

$$\mathcal{B}^\dagger(f^\dagger, \mathcal{S}^\dagger g) = \mathcal{A}^{\mathcal{D}}(\mathcal{S}^\dagger f^\dagger, \mathcal{S}^\dagger g^\dagger) = \mathcal{A}^{\mathcal{D}}(\mathcal{S}^\dagger g^\dagger, \mathcal{S}^\dagger f^\dagger) = \mathcal{B}^\dagger(g^\dagger, \mathcal{S}^\dagger f^\dagger).$$

Further, we state the following results regarding the additional regularity of the solution of (2.3), and consequently, for the eigenfunctions of $\mathcal{S}^\dagger$.

Theorem 2.1. *Let Ω be a polygonal domain with Lipschitz's boundary. Then for $f^\dagger \in H^\dagger$, there exists $s \in (1/2, 1]$ and $C > 0$ such that $\widetilde{u}^\dagger \in H^{2+s}(\Omega)$ and the following inequality holds*

$$\|\widetilde{u}^\dagger\|_{2+s,\Omega} \le C\, \|f^\dagger\|_{H^\dagger}. \tag{2.4}$$

Therefore, because of the compact inclusion $H^{2+s}(\Omega) \hookrightarrow H^\dagger$, $\mathcal{S}^\dagger$ is a compact operator. Thus, we conclude this section with the following spectral characterization result.

Theorem 2.2. *The spectrum of $\mathcal{S}^\dagger$ satisfies $sp(\mathcal{S}^\dagger) = \{0\} \cup \{\mu_k\}_{k\in\mathbb{N}}$, where $\{\mu_k\}_{k\in\mathbb{N}}$ is a sequence of positive eigenvalues which converges to 0, and the multiplicity of each eigenvalue is finite.*

3. Nonconforming virtual element discretization

In this section, we will recollect C^0-nonconforming virtual element method for the numerical approximation of the eigenvalue problems presented in (1.1a)–(1.1b) and (1.2a)–(1.2b) on general polygonal meshes. Nonconforming VEMs for biharmonic equation were first developed in the literature in Refs. [20,21]. Herein, we mainly follow the formulation of C^0-nonconforming VEM of Refs. [21]. The C^0-nonconforming VEM formulation of the variational formulation Problem 1 reads as

Problem 2. Find $(\lambda_h^\dagger, u_h^\dagger) \in \mathbb{R}\times\mathcal{V}_h$, with $u_h^\dagger \neq 0$ such that

$$\mathcal{A}_h^{\mathcal{D}}(u_h^\dagger, v_h) = \lambda_h^\dagger \mathcal{B}_h^\dagger(u_h^\dagger, v_h) \qquad \forall v_h \in \mathcal{V}_h.$$

In Problem 2, $(\lambda_h^\dagger, u_h^\dagger)$ is discrete approximation of $(\lambda^\dagger, u^\dagger)$, and $\mathcal{A}_h^{\mathcal{D}}(\cdot,\cdot)$, $\mathcal{B}_h^\dagger(\cdot,\cdot)$ are virtual element approximations of $\mathcal{A}^{\mathcal{D}}(\cdot,\cdot)$, $\mathcal{B}^\dagger(\cdot,\cdot)$, respectively. In the rest of the section, we introduce some notations to present the local and global nonconforming VEM spaces, and introduce some projectors on polynomial spaces to construct the discrete bilinear forms.

3.1. Mesh notations and regularity

Henceforth, we will denote by K a general polygon (even nonconvex, star shaped), by h_K and ∂K its diameter and boundary, respectively. Moreover, we denote by h_e the length of edge e. Let $\{\mathfrak{T}_h\}_{h>0}$ be a sequence of decompositions of Ω into general non-overlapping simple polygons K, where $h := \max_{K\in\mathfrak{T}_h} h_K$. We will denote the set of the edges in $\mathfrak{T}_h$ by $\mathcal{E}_h$, we decompose this set as $\mathcal{E}_h := \mathcal{E}_h^{\rm int} \cup \mathcal{E}_h^{\rm bdry}$, where $\mathcal{E}_h^{\rm int}$ and $\mathcal{E}_h^{\rm bdry}$ are the set of interior and boundary edges, respectively. Analogously, we will denote by $\mathfrak{E}_h := \mathfrak{E}_h^{\rm int} \cup \mathfrak{E}_h^{\rm bdry}$ the set of the all vertices in $\mathfrak{T}_h$, where $\mathfrak{E}_h^{\rm int}$ and $\mathfrak{E}_h^{\rm bdry}$ are the set of interior and boundary vertices, respectively. Besides, we will use the notation $\mathbf{n}_e$ and $\boldsymbol{t}_e$ for a unit normal and tangential vector of an edge $e \in \mathcal{E}_h$, respectively.

Moreover, we define the piecewise l-order polynomial space by:

$$\mathbb{P}_\ell(\mathfrak{T}_h) := \{q \in L^2(\Omega) : q|_K \in \mathbb{P}_\ell(K) \quad \forall K \in \mathfrak{T}_h\}.$$

Further, for all $m \in \mathbb{N} \cup \{0\}$, we recall the usual $L^2(K)$-projection onto the polynomial space $\mathbb{P}_m(K)$ by Π_K^m. Next, for any integer number $t > 0$, we introduce the following broken Sobolev space

$$H^t(\mathfrak{T}_h) := \{\phi \in L^2(\Omega) : \phi|_K \in H^t(K) \quad \forall K \in \mathfrak{T}_h\}$$

equipped with the following broken seminorm

$$|\phi|_{t,h} := \left(\sum_{K\in\mathfrak{T}_h} |\phi|^2_{t,K} \right)^{1/2}. \tag{3.1}$$

Upon recollecting [34], we define $[\![\phi]\!] := \phi^+ - \phi^-$, on each internal edge $e \in \mathcal{E}_h^{\rm int}$ for each function $\phi \in H^2(\mathfrak{T}_h)$, where $\phi^\pm$ denotes the trace of $\phi|_{K^\pm}$, with $e \subseteq \partial K^+ \cap \partial K^-$. For a boundary edge $e \in \mathcal{E}_h^{\rm bdry}$, the operator jump is define as: $[\![\phi]\!] := \phi|_e$. We introduce a subspace of $H^2(\mathfrak{T}_h)$ with weak continuity, given by:

$$\begin{aligned} H^{2,\rm NC}(\mathfrak{T}_h) := \Big\{ &\phi_h \in H^2(\mathfrak{T}_h) \cap H_0^1(\Omega) : \phi_h \text{ continuous at internal vertices}, \\ &\qquad \phi_h(\mathbf{v}_i) = 0 \quad \forall \mathbf{v}_i \in \mathfrak{E}_h^{\rm bdry}, \qquad \int_e [\![\partial_{\mathbf{n}_e}\phi_h]\!] = 0 \quad \forall e \in \mathcal{E}_h \Big\}. \end{aligned} \tag{3.2}$$

For the theoretical analysis, we suppose that $\mathfrak{T}_h$ satisfies the following assumptions:

Assumption 1 (*Mesh Regularity*). There exists a positive real number ρ independent of h such that for every $K \in \mathfrak{T}_h$, it holds that

(**A1**) **star-shapedness**: K is star-shaped with respect to an internal ball with radius bigger than ρh_K;
(**A2**) **uniform scaling**: the edge length h_e for all $e \in \mathcal{E}_h$ is bounded from below by ρh_K, i.e., $h_e \geq \rho h_K$.

Finally, we stress that we can decompose the continuous form defined in (2.1), as sum of elemental bilinear forms, $\mathcal{A}_K^{\mathcal{D}}(\cdot,\cdot) : H^2(K) \times H^2(K) \to \mathbb{R}$, $\mathcal{B}_K^{\dagger}(\cdot,\cdot) : H^{\dagger}(K) \times H^{\dagger}(K) \to \mathbb{R}$, such that

$$\mathcal{A}^{\mathcal{D}}(u,v) = \sum_{K\in\mathfrak{T}_h} \mathcal{A}_K^{\mathcal{D}}(u,v) \ \ \forall u,v \in H^2(\Omega); \qquad \mathcal{B}^{\dagger}(u,v) = \sum_{K\in\mathfrak{T}_h} \mathcal{B}_K^{\dagger}(u,v) \ \ \forall u,v \in H^{\dagger}(\Omega).$$

3.2. The local and global C^0-nonconforming virtual spaces

By employing the projection operator Π_K^m, we define the C^0-nonconforming virtual space. For every polygon $K \in \mathfrak{T}_h$, we introduce the following local virtual space:

$$\widetilde{\mathcal{V}}_h(K) := \left\{ \phi_h \in H^2(K) : \Delta^2\phi_h \in \mathbb{P}_2(K), \ \ \phi_h|_e \in \mathbb{P}_2(e), \ \ \Delta\phi_h|_e \in \mathbb{P}_0(e) \quad \forall e \subseteq \partial K \right\},$$

where Δ^2, and Δ are *Biharmonic* and *Laplace* operators. Then, we introduce three set of bounded linear functional. For a given $\phi_h \in \widetilde{\mathcal{V}}_h(K)$, we introduce the following set of linear operators.

- $(\mathbf{F_v})_{v\in\mathfrak{E}_h^K}$: the values of $\phi_h(\mathbf{v}_i)$ for all vertex $\mathbf{v}_i$ of the polygon K;
- $(\mathbf{F_e^1})_{e\in\mathcal{E}_h^K}$: the moments

$$\frac{1}{h_e}\int_e \phi_h \qquad \forall \text{ edge } e \in \mathcal{E}_h^K, \subseteq \partial K.$$

- $(\mathbf{F_e^2})_{e\in\mathcal{E}_h^K}$: the moments

$$\int_e \partial_{\mathbf{n}_e}\phi_h \qquad \forall\, \text{edge } e \in \mathcal{E}_h^K, \subseteq \partial K.$$

For each polygon K, we introduce the following elliptic projection operator $\Pi_K^{\mathcal{D}} : \widetilde{\mathcal{V}}_h(K) \longrightarrow \mathbb{P}_2(K) \subseteq \widetilde{\mathcal{V}}_h(K)$, as the solution of the following local problem:

$$\mathcal{A}_K^{\mathcal{D}}(\Pi_K^{\mathcal{D}} w_h, q_2) = \mathcal{A}_K^{\mathcal{D}}(w_h, q_2) \qquad \forall q_2 \in \mathbb{P}_2(K), \tag{3.3}$$

$$(\Pi_K^{\mathcal{D}} w_h, q_1)_{0,\partial K} = (w_h, q_1)_{0,\partial K} \qquad \forall q_1 \in \mathbb{P}_1(K), \tag{3.4}$$

where $(\cdot,\cdot)_{0,\partial K}$ denotes scalar product on $L^2(\partial K)$. Moreover, the projection $\Pi_K^{\mathcal{D}}\phi_h$ is computable from the DoFs associated with $\widetilde{\mathcal{V}}_h(K)$ (the proof can be seen in [35]).

Lemma 3.1. *The projection operator $\Pi_K^{\mathcal{D}} : \widetilde{\mathcal{V}}_h(K) \longrightarrow \mathbb{P}_2(K)$ is fully computable for every $w_h \in \widetilde{\mathcal{V}}_h(K)$, using only the information of the linear operators $(\mathbf{F_v})_{v\in\mathfrak{C}_h^K} - (\mathbf{F_e^2})_{e\in\mathcal{E}_h^K}$ of $w_h \in \widetilde{\mathcal{V}}_h(K)$.*

By employing the projection operator $\Pi_K^{\mathcal{D}}$, we introduce the enhanced nonconforming virtual space on each $K \in \mathfrak{T}_h$:

$$\mathcal{V}_h(K) := \left\{ v_h \in \widetilde{\mathcal{V}}_h(K) : (v_h - \Pi_K^{\mathcal{D}} v_h, q_2)_{0,K} = 0 \quad \forall q_2 \in \mathbb{P}_2(K) \right\}. \tag{3.5}$$

Based on the previous discussion, we summarize results in the following lemma.

Lemma 3.2.

- *The sets of linear operators $(\mathbf{F_v})_{v\in\mathfrak{C}_h^K} - (\mathbf{F_e^2})_{e\in\mathcal{E}_h^K}$ constitutes a set of DoFs for $\mathcal{V}_h(K)$;*
- *The operator $\Pi_K^{\mathcal{D}} : \mathcal{V}_h(K) \longrightarrow \mathbb{P}_2(K)$ is computable using the dofs $(\mathbf{F_v})_{v\in\mathfrak{C}_h^K} - (\mathbf{F_e^2})_{e\in\mathcal{E}_h^K}$;*
- *$\mathbb{P}_2(K) \subseteq \mathcal{V}_h(K)$.*

Now, for every decomposition $\mathfrak{T}_h$ of Ω into polygons K, we introduce the nonconforming global virtual space as follows:

$$\mathcal{V}_h := \left\{ v_h \in H^{2,\mathrm{NC}}(\mathfrak{T}_h) : v_h|_K \in \mathcal{V}_h(K) \quad \forall K \in \mathfrak{T}_h \right\}, \tag{3.6}$$

where the space $H^{2,\mathrm{NC}}(\mathfrak{T}_h)$ is defined in (3.2). It is observed that $\mathcal{V}_h \subseteq H^{2,\mathrm{NC}}(\mathfrak{T}_h) \subseteq H_0^1(\Omega)$ but $\mathcal{V}_h \nsubseteq H_0^2(\Omega)$. The formulation of discrete bilinear form associated with $\mathcal{B}_K^{\nabla}$ requires vector valued L^2 projection operator $\boldsymbol{\Pi}_K^1$ [36]. For future reference, we conventionally state the computability of the L^2-projection operators. Their proof can be found in [36], [37, Lemma 3.2].

Lemma 3.3.

- *For each $v_h \in \mathcal{V}_h(K)$, we have that the polynomial function $\Pi_K^2 v_h$ is computable using only the information of the dofs $(\mathbf{F_v})_{v\in\mathfrak{C}_h^K} - (\mathbf{F_e^2})_{e\in\mathcal{E}_h^K}$;*
- *For each scalar function $\phi_h \in \mathcal{V}_h(K)$, the linear vector polynomial $\boldsymbol{\Pi}_K^1 \nabla\phi_h$ is computable from the dofs $(\mathbf{F_v})_{v\in\mathfrak{C}_h^K} - (\mathbf{F_e^2})_{e\in\mathcal{E}_h^K}$ associated with ϕ_h.*

Remark 3.1. In this article, we have considered a general shape computational domain, including a nonconvex domain, and consequently, the eigenfunction solutions have fewer regularity [38]. The lowest order C^0- nonconforming space is employed to approximate the eigenvalues and eigenfunctions for **VEP** and **BEP**. Further, we derive the *a priori* estimates by using enriching operator which will be introduced in the forthcoming part of this article. However, if the exact eigenfunctions possess higher regularity, then we can generalize the convergence analysis by following similar arguments exploited in this article for any order of accuracy.

3.3. Construction of the bilinear forms

In this section, we will construct the discrete version of the continuous local bilinear forms defined in (2.1). With this end, we exploit the projection operators introduced in the previous section. Let $w_h, v_h \in \mathcal{V}_h(K)$. For each polygon K, we define the local discrete bilinear forms $\mathcal{A}^{\mathcal{D}}_{h,K}, \mathcal{B}^{0}_{h,K}, \mathcal{B}^{\nabla}_{h,K} : \mathcal{V}_h(K) \times \mathcal{V}_h(K) \longrightarrow \mathbb{R}$.

$$\mathcal{A}^{\mathcal{D}}_{h,K}(w_h, v_h) := \mathcal{A}^{\mathcal{D}}_{K}\big(\Pi^{\mathcal{D}}_K w_h, \Pi^{\mathcal{D}}_K v_h\big) + \mathcal{S}^{\mathcal{D}}_K\big((I-\Pi^{\mathcal{D}}_K)w_h, (I-\Pi^{\mathcal{D}}_K)v_h\big), \tag{3.7}$$

$$\mathcal{B}^{0}_{h,K}(w_h, v_h) := \mathcal{B}^{0}_{K}\big(\Pi^{2}_K w_h, \Pi^{2}_K v_h\big), \tag{3.8}$$

$$\mathcal{B}^{\nabla}_{h,K}(w_h, v_h) := \int_K \boldsymbol{\Pi}^1_K \nabla u_h \cdot \boldsymbol{\Pi}^1_K \nabla v_h, \tag{3.9}$$

where $\mathcal{S}^{\mathcal{D}}_K(\cdot,\cdot)$, be any symmetric positive definite bilinear form to be chosen as to satisfies:

$$c_* \mathcal{A}^{\mathcal{D}}_K(v_h, v_h) \le S^{\mathcal{D}}_K(v_h, v_h) \le c^* \mathcal{A}^{\mathcal{D}}_K(v_h, v_h) \qquad \forall v_h \in \mathcal{V}_h(K), \text{ with } \Pi^{\mathcal{D}}_K v_h = 0, \tag{3.10}$$

with c_* and c^* positive constants independent of h and K. In what follows, we will consider the following definition for the bilinear form $\mathcal{S}^{\mathcal{D}}_K(\cdot,\cdot)$:

$$\mathcal{S}^{\mathcal{D}}_K(w_h, v_h) := h_K^{-2} \sum_{i=1}^{N^K_{\text{dof}}} \text{dof}_i(w_h)\text{dof}_i(v_h) \tag{3.11}$$

for all $w_h, v_h \in \mathcal{V}_h(K)$, where N^K_{dof} denotes the number of DoFs of $\mathcal{V}_h(K)$ and dof_i is the operator that to each smooth enough function v associates the ith local degree of freedom $\text{dof}_i(v)$, with $1 \le i \le N^K_{\text{dof}}$.

Remark 3.2. We observe that, we have taken the Young modulus and the density of the plate, both equal to 1 (cf. (1.1)–(1.2)). For more realistic cases, we have to consider a multiplicative factor σ_K in front the stabilizer bilinear form $\mathcal{S}^{\mathcal{D}}_K(w_h, v_h)$ to take into account the magnitude of the material parameters. For instance, σ_K can be taken as the mean value of the eigenvalues of the local matrix $\mathcal{A}^{\mathcal{D}}_K\big(\Pi^{\mathcal{D}}_K w_h, \Pi^{\mathcal{D}}_K v_h\big)$.

The following result establishes that $\mathcal{S}^{\mathcal{D}}_K(\cdot,\cdot)$ satisfies the stability property (3.10). The proof follows the arguments presented in [39,40]. We omit further details since the proof is beyond the scopes of the present paper.

Proposition 3.1. *The bilinear form defined in (3.11) satisfies the stability property (3.10).*

The global forms $\mathcal{A}^{\mathcal{D}}_h, \mathcal{B}^{\dagger}_h : \mathcal{V}_h \times \mathcal{V}_h \longrightarrow \mathbb{R}$ are defined as sum of elemental forms such as

$$\mathcal{A}^{\mathcal{D}}_h(w_h, v_h) = \sum_{K \in \mathfrak{T}_h} \mathcal{A}^{\mathcal{D}}_{h,K}(w_h, v_h); \quad \mathcal{B}^{\dagger}_h(w_h, v_h) = \sum_{K \in \mathfrak{T}_h} \mathcal{B}^{\dagger}_{h,K}(w_h, v_h). \tag{3.12}$$

The following result establishes the usual consistency and stability properties for the discrete local forms.

Proposition 3.2. *The local bilinear forms $\mathcal{A}^{\mathcal{D}}_{h,K}$, $\mathcal{B}^{\dagger}_{h,K}(\cdot,\cdot)$, on each element K satisfy*

- *Consistency: for all $h > 0$ and for all $K \in \mathfrak{T}_h$, we have that*

$$\mathcal{A}^{\mathcal{D}}_{h,K}(v_h, q_2) = \mathcal{A}^{\mathcal{D}}_K(v_h, q_2), \quad \mathcal{B}^{\dagger}_{h,K}(v_h, q_2) = \mathcal{B}^{\dagger}_K(v_h, q_2) \quad \forall (v_h, q_2) \in \mathcal{V}_h(K) \times \mathbb{P}_2(K).$$

- *Stability and boundedness: There exist positive constants $\alpha_i, i = 1, \ldots, 4$ independent of K, such that:*

$$\alpha_1 \mathcal{A}^{\mathcal{D}}_K(v_h, v_h) \le \mathcal{A}^{\mathcal{D}}_{h,K}(v_h, v_h) \le \alpha_2 \mathcal{A}^{\mathcal{D}}_K(v_h, v_h) \qquad \forall v_h \in \mathcal{V}_h(K), \tag{3.13}$$

$$\mathcal{B}^{0}_{h,K}(v_h, v_h) \le \alpha_3 \|v_h\|^2_{0,K} \qquad \forall v_h \in \mathcal{V}_h(K), \tag{3.14}$$

$$\mathcal{B}^{\nabla}_{h,K}(v_h, v_h) \le \alpha_4 \|v_h\|^2_{1,K} \qquad \forall v_h \in \mathcal{V}_h(K). \tag{3.15}$$

Proof. The consistency property follows from the definition the bilinear forms. Then, (3.13) follows from Proposition 3.1, and (3.14) and (3.15) are consequence of the stability of the L^2-projection operators Π^2_K and $\boldsymbol{\Pi}^1_K$, respectively. □

Remark 3.3. To prove Proposition 3.2, we have assumed certain regularity of the polygonal mesh in Assumption 1, where the edge length h_e is comparable with the diameter of polygon K. We stress that the particular choice of the stabilizer given in (3.11) satisfies the condition as mentioned in (3.10). However, the closed forms of stabilizers associated with the biharmonic operator are not straightforward in the presence of arbitrary small edges in the discretization, i.e., when (**A2**) is violated (cf. Assumption 1). Some remarkable analysis have been proposed in this direction for C^0 conforming VEM space [41,42]. The explicit forms of the stabilizers for C^1 VEM and nonconforming VEM for biharmonic operators without the mesh regularity assumption, i.e., (**A2**) are still open problems in the VEM literature.

Remark 3.4. In this article, we have offered C^0-nonconforming virtual element schemes for both **VEP** and **BEP** on convex and more general nonconvex domain. Further, to approximate the right hand side bilinear forms such as $(u, v)_{0,\Omega}$, or $(\nabla u, \nabla v)_{0,\Omega}$, we have employed polynomial projection operators and considered only computable polynomial part of the discretization. The above mentioned discretization helps to estimate the convergence of discrete solution operator to continuous operator in the norm of continuous space, and consequently the convergence of eigenvalues and eigenfuctions are concluded by directly using Babuška–Osborn theory [31]. However, one can discretize the bilinear forms such as $(u, v)_{0,\Omega}$, or $(\nabla u, \nabla v)_{0,\Omega}$, by considering polynomial and non-polynomial parts, and their convergence analysis can be derived by exploiting Descloux–Nassif–Rappaz theory [43,44].

In order to study the discrete eigenvalue problems (cf. Problem 2), we state the following result which establishes that $|\cdot|_{2,h}$ (cf. (3.1)) is a norm in $\mathcal{V}_h$. An application of Poincaré inequality and boundary condition of the space yield the following assertion. The proof is established in [20, Lemma 5.1].

Lemma 3.4. *For all $v_h \in \mathcal{V}_h$, there exists a positive constant C independent of h such that the following inequality holds true:*

$$\|v_h\|_{0,\Omega} + |v_h|_{1,\Omega} \leq C|v_h|_{2,h}.$$

The following result establishes some properties for the discrete forms $\mathcal{A}_h^{\mathcal{D}}(\cdot,\cdot)$, $\mathcal{B}_h^0(\cdot,\cdot)$ and $\mathcal{B}_h^{\nabla}(\cdot,\cdot)$ which will be used to conclude the well-posedness of the discrete source problem associated with Problem 2. The proof follows from the definition of the respective forms.

Lemma 3.5. *For all $w_h, v_h \in \mathcal{V}_h$, there exist positive constants $C_1, \widetilde{\alpha}$, independent of h, such that*

$$|\mathcal{A}_h^{\mathcal{D}}(w_h, v_h)| \leq C_1\, |w_h|_{2,h}|v_h|_{2,h}; \qquad |\mathcal{B}_h^0(w_h, v_h)| \leq C_1\, |w_h|_{2,h}|v_h|_{2,h}; \tag{3.16}$$

$$|\mathcal{B}_h^{\nabla}(w_h, v_h)| \leq C_1\, |w_h|_{2,h}|v_h|_{2,h}; \qquad \mathcal{A}_h^{\mathcal{D}}(v_h, v_h) \geq \widetilde{\alpha}|v_h|_{2,h}^2. \tag{3.17}$$

Further, we define the discrete versions of the solution operators $\mathcal{S}^\dagger$ (cf. (2.3)) and associated with the discrete spectral Problem 2 as follows:

$$\mathcal{S}_h^\dagger : H^\dagger \to \mathcal{V}_h \subset H^\dagger$$
$$f^\dagger \longmapsto \mathcal{S}_h^\dagger f^\dagger =: \widetilde{u}_h^\dagger,$$

where $\widetilde{u}_h^\dagger$ is the unique solution of the following source problem

$$\mathcal{A}_h^{\mathcal{D}}(\widetilde{u}_h^\dagger, v_h) = \mathcal{B}_h^\dagger(f^\dagger, v_h) \qquad \forall v_h \in \mathcal{V}_h. \tag{3.18}$$

From Lemma 3.5 and Lax–Milgram we have that the discrete solution operator $\mathcal{S}_h^\dagger$ are well defined and bounded. In fact, we assert that

$$|\widetilde{u}_h^\dagger|_{2,h} \leq C\|f^\dagger\|_{H^\dagger} \qquad \forall f^\dagger \in H^\dagger,$$

where the positive constant C is independent of h. It is easy to check that $(\lambda_h^\dagger, u_h^\dagger) \in \mathbb{R}\times\mathcal{V}_h$ is a solution of Problem 2 if and only if $(\mu_h^\dagger, u_h^\dagger) \in \mathbb{R}\times\mathcal{V}_h$ with $\mu_h^\dagger := \frac{1}{\lambda_h^\dagger}$ is an eigenpair of $\mathcal{S}_h^\dagger$. Moreover from the definition of $\mathcal{A}_h^{\mathcal{D}}(\cdot,\cdot)$ and $\mathcal{B}_h^\dagger(\cdot,\cdot)$, we can validate that $\mathcal{S}_h^\dagger$ is self-adjoint.

We finish this section with the spectral characterization for operators $\mathcal{S}_h^\dagger$.

Theorem 3.1. *Let m_h and z_h be the dimensions of the discrete spaces $\mathcal{V}_h$ and $Z_h := \{u_h \in \mathcal{V}_h : \mathcal{B}_h^{\nabla}(u_h, v_h) = 0 \quad \forall v_h \in \mathcal{V}_h\}$. Then, the following results hold:*

(i) The spectrum of $\mathcal{S}_h^0$ consists of m_h real and positive eigenvalues repeated according to their multiplicities.
(ii) The spectrum of $\mathcal{S}_h^{\nabla}$ consists of $m_h - z_h$ real and positive eigenvalues repeated according to their multiplicities.

4. A priori error estimates for the source problems

In this subsection, we first introduce some specific theoretical tools and characterization that will be used for theoretical estimates. Since, we are interested to derive convergence analysis of source problem (2.3) on nonconvex domain, we will introduce *E*nriching operator, say, E_h from C^0-nonconforming space to its C^1 conforming counter space. Herein, we briefly define E_h and related approximation properties of E_h.

Conforming virtual local space. For every polygon $K \in \mathfrak{T}_h$, we introduce the following preliminary finite dimensional space [6,39]:

$$\widetilde{\mathcal{V}}_h^{\mathrm{C}}(K) := \big\{\phi_h \in H^2(K) : \Delta^2\phi_h \in \mathbb{P}_2(K), \phi_h|_{\partial K} \in C^0(\partial K), \phi_h|_e \in \mathbb{P}_3(e)\ \forall e \subseteq \partial K,$$
$$\nabla\phi_h|_{\partial K} \in [C^0(\partial K)]^2, \partial_{\mathbf{n}_e}\phi_h|_e \in \mathbb{P}_1(e)\ \forall e \subseteq \partial K\big\},$$

Next, for a given $\phi_h \in \widetilde{\mathcal{V}}_h^{\mathrm{C}}(K)$, we introduce two sets $(\mathbf{F}^{\mathbf{c}}_{\mathbf{v}})_{\mathbf{v}\in\mathfrak{E}_h^K}$ and $(\mathbf{F}^{\mathbf{c}}_{\mathbf{v},\nabla})_{\mathbf{v}\in\mathfrak{E}_h^K}$ of linear operators from the local virtual space $\widetilde{\mathcal{V}}_h^{\mathrm{C}}(K)$ into $\mathbb{R}$:

- $(\mathbf{F}^{\mathbf{c}}_{\mathbf{v}})_{\mathbf{v}\in\mathfrak{E}_h^K}$: the values of $\phi_h(\mathbf{v})$ for all vertex $\mathbf{v} \in \partial K$,
- $(\mathbf{F}^{\mathbf{c}}_{\mathbf{v},\nabla})_{\mathbf{v}\in\mathfrak{E}_h^K}$: the values of $h_{\mathbf{v}}\partial_j\phi_h(\mathbf{v})$ for all vertex $\mathbf{v} \in \partial K$, and $j = 1, 2$,

where $h_{\mathbf{v}}$ is a characteristic length attached to each vertex $\mathbf{v}$, for instance to the maximum diameter of the elements with $\mathbf{v}$ as a vertex. Now, we consider the operator $\Pi_K^{\mathcal{D},\mathrm{C}} : \widetilde{\mathcal{V}}_h^{\mathrm{C}}(K) \longrightarrow \mathbb{P}_2(K) \subseteq \widetilde{\mathcal{V}}_h^{\mathrm{C}}(K)$ associated to the conforming approach, which is computable using the sets $\mathbf{F}^{\mathbf{c}}_{\mathbf{v}}$ and $\mathbf{F}^{\mathbf{c}}_{\mathbf{v},\nabla}$ (for more details see [45, Lemma 2.1]). Next, for each $K \in \mathfrak{T}_h$, we introduce the conforming local enhanced virtual space as follows:

$$\mathcal{V}_h^{\mathrm{C}}(K) := \left\{\phi_h \in \widetilde{\mathcal{V}}_h^{\mathrm{C}}(K) : (\phi_h - \Pi_K^{\mathcal{D},\mathrm{C}}\phi_h, q)_{0,K} = 0 \quad \forall q \in \mathbb{P}_2(K)\right\}. \tag{4.1}$$

In this space the sets $\mathbf{F}^{\mathbf{c}}_{\mathbf{v}}$ and $\mathbf{F}^{\mathbf{c}}_{\mathbf{v},\nabla}$ constitute a set of degrees of freedom.

Conforming virtual global space. For every decomposition $\mathfrak{T}_h$ of Ω into polygons K, we define the conforming virtual spaces $\mathcal{V}_h^{\mathrm{C}}$:

$$\mathcal{V}_h^{\mathrm{C}} := \left\{\phi_h \in \mathcal{V} :\ \phi_h|_K \in \mathcal{V}_h^{\mathrm{C}}(K) \qquad \forall K \in \mathfrak{T}_h\right\}. \tag{4.2}$$

For a vertex $\mathbf{v} \in \mathfrak{E}_h$, we denote by $\mathfrak{A}(\mathbf{v})$ the union of all elements in $\mathfrak{T}_h$, sharing the vertex $\mathbf{v}$ and by $N(\mathbf{v})$ the number of elements of $\mathfrak{A}(\mathbf{v})$. For any $\varphi_h \in \mathcal{V}_h$, we introduce the piecewise L^2-projection Π^2, as follows:

$$\Pi^2\varphi_h|_K = \Pi_K^2(\varphi_h|_K),$$

where Π_K^2 is the L^2-projection from $\mathcal{V}_h(K)$ onto $\mathbb{P}_2(K)$ (cf. Lemma 3.3) and $\mathcal{V}_h(K)$ is the local nonconforming virtual space defined in (3.5). For each function $\varphi_h \in \mathcal{V}_h$, the function $E_h\varphi_h \in \mathcal{V}_h^{\mathrm{C}}$ in the conforming counterpart will be constructed as follows:

$$E_h(\varphi_h)(x) = \sum_{i=1}^{N_{\mathrm{dof}}^{\mathrm{C}}} F_i^c(E_h(\varphi_h))\chi_i(x),$$

where the functions $\{\chi_i\}_{i=1}^{N_{\mathrm{dof}}^{\mathrm{C}}}$ are the set of shape basis functions associated to space $\mathcal{V}_h^{\mathrm{C}}$ and $N_{\mathrm{dof}}^{\mathrm{C}} := \dim(\mathcal{V}_h^{\mathrm{C}})$. More precisely, the values of degrees of freedom for the enriching operator are determined as follows:

1. For the values at interior vertices $\mathbf{v} \in \mathfrak{E}_h^{\mathrm{int}}$, we consider:
$$F_{\mathbf{v}}^c(E_h\varphi_h) := \frac{1}{N(\mathbf{v})}\sum_{\widetilde{K}\in\mathfrak{A}(\mathbf{v})} \Pi^2\varphi_h|_{\widetilde{K}}(\mathbf{v}).$$
2. For the gradient values at interior vertices $\mathbf{v} \in \mathfrak{E}_h^{\mathrm{int}}$, we consider:
$$F_{\mathbf{v},\nabla}^c(E_h\varphi_h) := \frac{1}{N(\mathbf{v})}\sum_{\widetilde{K}\in\mathfrak{A}(\mathbf{v})} h_{\mathbf{v}}\partial_j(\Pi^2\varphi_h|_{\widetilde{K}})(\mathbf{v}) \quad \forall j \in \{1, 2\}.$$

The approximation property of the operator E_h are provided in [37, Section 4.2]. Consequently, we merely recollect the results in the following Lemma.

Lemma 4.1.

- *For all $v_h \in \mathcal{V}_h$, there exists $C > 0$ independent of h, such that*

$$\|v_h - E_h v_h\|_{0,\Omega} + h|v_h - E_h v_h|_{1,\Omega} + h^2|E_h v_h|_{2,\Omega} \leq Ch^2|v_h|_{2,h};$$

- *Let $w \in H^{2+t}(\Omega)$, with $t \in [0, 1]$. Then, for all $v_h \in \mathcal{V}_h$ we have*

$$\mathcal{A}^{\mathcal{D}}(w, v_h - E_h v_h) \leq Ch^t\|w\|_{2+t,\Omega}|v_h|_{2,h}.$$

By employing enriching operator, we will establish an error estimate in broken H^2-norm for the solution of the continuous and discrete sources problems. First, we start noticing that for all $v_h \in \mathcal{V}_h$ the consistency error in the source problem (also called nonconformity error) is defined as follow. For any $f^\dagger \in H^\dagger$, let $\mathcal{N}_h(\widetilde{u}^\dagger, \cdot) : \mathcal{V}_h \to \mathbb{R}$ be the functional given by

$$\mathcal{N}_h(\widetilde{u}^\dagger, v_h) := \sum_{K\in\mathfrak{T}_h} \mathcal{A}_K^{\mathcal{D}}(\widetilde{u}^\dagger, v_h) - \mathcal{B}^\dagger(f^\dagger, v_h) \qquad \forall v_h \in \mathcal{V}_h, \tag{4.3}$$

where $\widetilde{u}^\dagger \in H^{2+s}(\Omega) \cap \mathcal{V}$ is the unique solution of problem (2.3). Moreover, we have the following estimation for the consistency error $\mathcal{N}_h(\widetilde{u}^\dagger, \cdot)$ defined above. Their proof can be obtained by employing arguments as [37, Lemma 4.12].

Lemma 4.2. *Given $f^\dagger \in H^\dagger$, let $\widetilde{u}^\dagger$ be the solution of the source problem (2.3). Then, for all $v_h \in \mathcal{V}_h$, there exists a constant $C > 0$ independent to h, such that*

$$\mathcal{N}_h(\widetilde{u}^\dagger, v_h) \leq Ch^s(\|\widetilde{u}^\dagger\|_{2+s,\Omega} + \|f^\dagger\|_{H^\dagger})|v_h|_{2,h},$$

where $\mathcal{N}_h(\widetilde{u}^\dagger, \cdot)$ is the consistency error defined by the relation (4.3) and $\widetilde{u}^\dagger \in H^{2+s}(\Omega) \cap \mathcal{V}$ (cf. Theorem 2.1).

We have the following approximation result in the virtual space $\mathcal{V}_h$ (see [20,23,46]).

Proposition 4.1. *Assume that $\mathbf{A_1} - \mathbf{A_2}$ are satisfied. Then, for each $w \in H^{2+t}(\Omega)$, with $t \in [0, 1]$, there exist $w_I \in \mathcal{V}_h$ and $C > 0$, independent of h, such that*

$$\|w - w_I\|_{\ell,K} \leq Ch_K^{2+t-\ell}|w|_{2+t,K}, \qquad \ell = 0, 1, 2.$$

In what follows we will prove some preliminary results in order to establish that the operator $\mathcal{S}_h^\dagger$ converges to $\mathcal{S}^\dagger$, when h goes to zero. First, we have the following Strang-type result.

Lemma 4.3. *Assume the mesh assumptions $\mathbf{A_1} - \mathbf{A_2}$. Given $f^\dagger \in H^\dagger$ let $\widetilde{u}^\dagger$ and $\widetilde{u}_h^\dagger$ be the unique solutions of the source problems (2.3) and (3.18), respectively. Then, for each approximation $\widetilde{u}_I^\dagger$ of $\widetilde{u}^\dagger$ in $\mathcal{V}_h$ and for every approximation $\widetilde{u}_\pi^\dagger$ of $\widetilde{u}^\dagger$ in $\mathbb{P}_2(\mathfrak{T}_h)$, there exists $C > 0$, independent of h, such that*

$$|\widetilde{u}^\dagger - \widetilde{u}_h^\dagger|_{2,h} \leq C\left(|\widetilde{u}^\dagger - \widetilde{u}_I^\dagger|_{2,h} + |\widetilde{u}^\dagger - \widetilde{u}_\pi^\dagger|_{2,h} + \sup_{\substack{v_h\in\mathcal{V}_h\\ v_h\neq 0}} \frac{|\mathcal{B}_h^\dagger(f^\dagger, v_h) - \mathcal{B}^\dagger(f^\dagger, v_h)|}{|v_h|_{2,h}} + \sup_{\substack{v_h\in\mathcal{V}_h\\ v_h\neq 0}} \frac{\mathcal{N}_h(\widetilde{u}^\dagger, v_h)}{|v_h|_{2,h}}\right).$$

Proof. Let $\widetilde{u}_I^\dagger \in \mathcal{V}_h$ be the interpolant of $\widetilde{u}^\dagger$ such that Proposition 4.1 holds true. We set $\delta_h := \widetilde{u}_h^\dagger - \widetilde{u}_I^\dagger \in \mathcal{V}_h$. Then,

$$|\widetilde{u}^\dagger - \widetilde{u}_h^\dagger|_{2,h} \leq |\widetilde{u}^\dagger - \widetilde{u}_I^\dagger|_{2,h} + |\delta_h|_{2,h}. \tag{4.4}$$

By using the coercivity property of $\mathcal{A}_h^{\mathcal{D}}(\cdot, \cdot)$ (cf. Lemma 3.5) and the consistency of bilinear form $\mathcal{A}_{h,K}^{\mathcal{D}}(\cdot, \cdot)$ (cf. Proposition 3.2), we have

$$\begin{aligned}\widetilde{\alpha}|\delta_h|_{2,h}^2 &\leq \mathcal{A}_h^{\mathcal{D}}(\delta_h, \delta_h) = \mathcal{A}_h^{\mathcal{D}}(\widetilde{u}_h^\dagger, \delta_h) - \mathcal{A}_h^{\mathcal{D}}(\widetilde{u}_I^\dagger, \delta_h)\\ &= \mathcal{B}_h^\dagger(f^\dagger, \delta_h) - \mathcal{B}^\dagger(f^\dagger, \delta_h) - \mathcal{N}_h(\widetilde{u}^\dagger, \delta_h) - \sum_{K\in\mathfrak{T}_h} \mathcal{A}_{h,K}^{\mathcal{D}}(\widetilde{u}_I^\dagger - \widetilde{u}_\pi^\dagger, \delta_h) + \sum_{K\in\mathfrak{T}_h} \mathcal{A}_K^{\mathcal{D}}(\widetilde{u}^\dagger - \widetilde{u}_\pi^\dagger, \delta_h).\end{aligned}$$

Then we get

$$|\delta_h|_{2,h} \leq C\Big(|\widetilde{u}^\dagger - \widetilde{u}_I^\dagger|_{2,h} + |\widetilde{u}^\dagger - \widetilde{u}_\pi^\dagger|_{2,h} + \sup_{\substack{v_h \in \mathcal{V}_h \\ v_h \neq 0}} \frac{|\mathcal{B}_h^\dagger(f^\dagger, v_h) - \mathcal{B}^\dagger(f^\dagger, v_h)|}{|v_h|_{2,h}} + \sup_{\substack{v_h \in \mathcal{V}_h \\ v_h \neq 0}} \frac{\mathcal{N}_h(u, v_h)}{|v_h|_{2,h}}\Big). \tag{4.5}$$

Thus, from (4.4) and (4.5), we conclude the proof. □

Next, we will present an important approximation result for polynomials on star-shaped domains to be used in the Strang-type estimate (see, for instance [23,47]).

Proposition 4.2. *Assume that* $\mathbf{A_1} - \mathbf{A_1}$ *are satisfied. Then, for every* $w \in H^{2+t}(K)$*, with* $t \in [0, 1]$*, there exist* $w_h \in \mathbb{P}_2(K)$ *and* $C > 0$*, independent of* h*, such that*

$$\|w - w_\pi\|_{\ell,K} \leq C h_K^{2+t-\ell} |w|_{2+t,K}, \qquad \ell = 0, 1, 2.$$

We have the following estimation involving the continuous and discrete functionals.

Proposition 4.3. *Assume the assumption* $\mathbf{A_1} - \mathbf{A_2}$*. For all* $f^\dagger \in H^\dagger$ *there exists a positive constant* C *independent of the parameter* h *such that the following estimates hold true:*

$$\sup_{\substack{v_h \in \mathcal{V}_h \\ v_h \neq 0}} \frac{|\mathcal{B}_h^0(f^0, v_h) - \mathcal{B}^0(f^0, v_h)|}{|v_h|_{2,h}} \leq C h^2 \|f^0\|_{0,\Omega}, \tag{4.6}$$

$$\sup_{\substack{v_h \in \mathcal{V}_h \\ v_h \neq 0}} \frac{|\mathcal{B}_h^\nabla(f^\nabla, v_h) - \mathcal{B}^\nabla(f^\nabla, v_h)|}{|v_h|_{2,h}} \leq C h \|f^\nabla\|_{1,\Omega}. \tag{4.7}$$

Proof. The proof can be obtained from the definitions of the bilinear form $\mathcal{B}_h^\dagger(\cdot,\cdot)$ together with consistency property formally stated in Propositions 3.2, and 4.2. □

As a consequence, we obtain the following theorem, which provides the rate of convergence of our virtual element scheme.

Theorem 4.1. *Assume the mesh assumptions* $\mathbf{A_1} - \mathbf{A_2}$*. Given* $f^\dagger \in H^\dagger$ *let* $\widetilde{u}^\dagger$ *and* $\widetilde{u}_h^\dagger$ *be the unique solutions of the source problems (2.3) and (3.18), respectively. Then, for each approximation* $\widetilde{u}_I^\dagger$ *of* $\widetilde{u}^\dagger$ *in* $\mathcal{V}_h$ *and for every approximation* $\widetilde{u}_\pi^\dagger$ *of* $\widetilde{u}^\dagger$ *in* $\mathbb{P}_2(\mathfrak{T}_h)$*, there exists* $C > 0$*, independent of* h*, such that*

$$|\widetilde{u}^\dagger - \widetilde{u}_h^\dagger|_{2,h} \leq C h^s (\|\widetilde{u}^\dagger\|_{2+s,\Omega} + \|f^\dagger\|_{H^\dagger}) \leq C h^s \|f^\dagger\|_{H^\dagger}, \tag{4.8}$$

where $s \in (1/2, 1]$ *is such that* $\widetilde{u}^\dagger \in H^{2+s}(\Omega) \cap H_0^2(\Omega)$ *(cf. Theorem 2.1).*

Proof. The estimate (4.8) follows by combining Lemma 4.3, Propositions 4.1, 4.2, 4.3 and Lemma 4.2. □

4.1. Error estimates in L^2 and H^1 norms for the source problems

In this section, we would like to derive the error estimates of source problem (2.3), in H^1 and L^2 norms. The results are based on the so-called duality argument. Moreover, we recollect one major result which will be used to derive the error estimates for the approximation of eigenvalues and eigenfunctions. Their proof can be found in [37, Lemma 4.11].

Lemma 4.4. *For* $\phi \in H^{2+t}(\Omega)$ *and* $v \in H^{2+t}(\Omega) \cap H_0^2(\Omega)$*, with* $t \in [0, 1]$*, it holds:*

$$\mathcal{A}^{\mathcal{D}}(\phi, v - v_I) \leq C\, h^{2t} \|\phi\|_{2+t,\Omega} \|v\|_{2+t,\Omega}, \tag{4.9}$$

where v_I *is the interpolant of* v *in the virtual space* $\mathcal{V}_h$*.*

Now, we focus to derive primary result of this section.

Theorem 4.2. *Assume the mesh assumptions* $\mathbf{A_1} - \mathbf{A_2}$. *Given* $f^\dagger \in H^\dagger$ *let* $\widetilde{u}^\dagger$ *and* $\widetilde{u}_h^\dagger$ *be the unique solutions of the source problems* (2.3) *and* (3.18)*, respectively. Then, for each approximation* $\widetilde{u}_I^\dagger$ *of* $\widetilde{u}^\dagger$ *in* $\mathcal{V}_h$ *and for every approximation* $\widetilde{u}_\pi^\dagger$ *of* $\widetilde{u}^\dagger$ *in* $\mathbb{P}_2(\mathfrak{T}_h)$*, there exists* $C > 0$*, independent of* h*, such that*

$$\|\widetilde{u}^\dagger - \widetilde{u}_h^\dagger\|_{0,\Omega} + \|\widetilde{u}^\dagger - \widetilde{u}_h^\dagger\|_{1,\Omega} \le Ch^{2s}(\|\widetilde{u}^\dagger\|_{2+s,\Omega} + \|f^\dagger\|_{H^\dagger}) \le Ch^{2s}\|f^\dagger\|_{H^\dagger}, \tag{4.10}$$

where $s \in (1/2, 1]$ *is such that* $\widetilde{u}^\dagger \in H^{2+s}(\Omega) \cap H_0^2(\Omega)$ *(cf. Theorem* 2.1*).*

Proof. In order to prove the H^1 estimate in (4.10), let $\widetilde{u}_I^\dagger \in \mathcal{V}_h$ be the interpolant of $\widetilde{u}^\dagger$ such that Proposition 4.1 holds true. We set $\delta_h := (\widetilde{u}_h^\dagger - \widetilde{u}_I^\dagger) \in \mathcal{V}_h$. Then, we write

$$\widetilde{u}_h^\dagger - \widetilde{u}^\dagger = (\widetilde{u}_h^\dagger - \widetilde{u}_I^\dagger) + (\widetilde{u}_I^\dagger - \widetilde{u}^\dagger) = (\widetilde{u}_I^\dagger - \widetilde{u}^\dagger) + (\delta_h - E_h\delta_h) + E_h\delta_h.$$

Thus, by using the triangle inequality together Proposition 4.1, Lemma 4.1 and Theorem 4.1, we have

$$\begin{aligned}
|\widetilde{u}^\dagger - \widetilde{u}_h^\dagger|_{1,\Omega} &\le |\widetilde{u}^\dagger - \widetilde{u}_I^\dagger|_{1,\Omega} + |\delta_h - E_h\delta_h|_{1,\Omega} + |E_h\delta_h|_{1,\Omega} \\
&\le C\big(h^{1+s}\|\widetilde{u}^\dagger\|_{2+s} + h|\delta_h|_{2,h} + |E_h\delta_h|_{1,\Omega}\big) \\
&\le Ch^{1+s}\|\widetilde{u}^\dagger\|_{2+s,\Omega} + \|\nabla E_h\delta_h\|_{0,\Omega} \\
&\le Ch^{2s}\|\widetilde{u}^\dagger\|_{2+s,\Omega} + \|\nabla E_h\delta_h\|_{0,\Omega}.
\end{aligned} \tag{4.11}$$

In what follows, we will estimate the term $\|\nabla E_h\delta_h\|_{0,\Omega}$. To do that, we consider the following auxiliary problem: find $\phi \in \mathcal{V}$, such that

$$\mathcal{A}^{\mathcal{D}}(w, \phi) = \int_\Omega \nabla(E_h\delta_h) \cdot \nabla w \qquad \forall w \in \mathcal{V}, \tag{4.12}$$

where the bilinear form $\mathcal{A}^{\mathcal{D}}(\cdot,\cdot)$ is defined in (2.1). From Theorem 2.1, we have that $\phi \in H^{2+s}(\Omega) \cap \mathcal{V}$ and

$$\|\phi\|_{2+s,\Omega} \le C\|\nabla E_h\delta_h\|_{0,\Omega}. \tag{4.13}$$

where $C > 0$ is a constant independent of h.

Then, taking $w = E_h\delta_h \in \mathcal{V}_h^{\mathrm{C}} \subset \mathcal{V}$ as test function ($\mathcal{V}_h^{\mathrm{C}}$ is lowest order C^1 conforming VEM space defined in [39]), adding and subtracting δ_h in problem (4.12), we obtain

$$\|\nabla E_h\delta_h\|_{0,\Omega}^2 = \mathcal{A}^{\mathcal{D}}(E_h\delta_h, \phi) = \mathcal{A}^{\mathcal{D}}(E_h\delta_h - \delta_h, \phi) + \mathcal{A}^{\mathcal{D}}(\delta_h, \phi) =: T_1 + T_2. \tag{4.14}$$

We will estimate the terms T_1 and T_2 in the above identity. Indeed, for the T_1, we use the definition of bilinear form $\mathcal{A}^{\mathcal{D}}(\cdot,\cdot)$, Proposition 4.1, together with second asset of Lemma 4.1, Theorem 4.1 and the triangle inequality, to obtain

$$T_1 = \mathcal{A}^{\mathcal{D}}(E_h\delta_h - \delta_h, \phi) \le Ch^s|\delta_h|_{2,h}\|\phi\|_{2+s,\Omega} \le Ch^{2s}\|\widetilde{u}^\dagger\|_{2+s,\Omega}\|\phi\|_{2+s,\Omega}.$$

Then, from the above estimate and (4.13), we obtain

$$T_1 \le Ch^{2s}(\|\widetilde{u}^\dagger\|_{2+s,\Omega} + \|f^\dagger\|_{H^\dagger})\|\nabla E_h\delta_h\|_{0,\Omega}. \tag{4.15}$$

To bound the term T_2, we consider $\phi_I \in \mathcal{V}_h$ the interpolant of ϕ such that Proposition 4.1 holds true. Then, rewriting $\delta_h = (\widetilde{u}_h^\dagger - \widetilde{u}^\dagger) + (\widetilde{u}^\dagger - \widetilde{u}_I^\dagger)$, adding and subtracting ϕ_I, and using the bilinearity of form $\mathcal{A}^{\mathcal{D}}(\cdot,\cdot)$, we obtain

$$\begin{aligned}
T_2 &:= \mathcal{A}^{\mathcal{D}}(\delta_h, \phi) = \mathcal{A}^{\mathcal{D}}(\widetilde{u}^\dagger - \widetilde{u}_I^\dagger, \phi) + \mathcal{A}^{\mathcal{D}}(\widetilde{u}_h^\dagger - \widetilde{u}^\dagger, \phi - \phi_I) + \mathcal{A}^{\mathcal{D}}(\widetilde{u}_h^\dagger - \widetilde{u}^\dagger, \phi_I) \\
&= T_2^a + T_2^b + T_2^c.
\end{aligned} \tag{4.16}$$

Now, we will estimate each term in (4.16). Indeed, we use again the definition of bilinear form $\mathcal{A}^{\mathcal{D}}(\cdot,\cdot)$ and Lemma 4.4 to obtain

$$T_2^a \le Ch^{2s}\|\phi\|_{2+s,\Omega}\|\widetilde{u}^\dagger\|_{2+s,\Omega} \le Ch^{2s}\|\widetilde{u}^\dagger\|_{2+s,\Omega}\|\nabla E_h\delta_h\|_{0,\Omega}. \tag{4.17}$$

For T_2^b, we use the continuity of bilinear form $\mathcal{A}^{\mathcal{D}}(\cdot,\cdot)$, Proposition 4.1, Theorem 4.1 and (4.13), to get

$$T_2^b := \mathcal{A}^{\mathcal{D}}(\widetilde{u}_h^\dagger - \widetilde{u}^\dagger, \phi - \phi_I) \le Ch^{2s}(\|\widetilde{u}^\dagger\|_{2+s,\Omega} + \|f^\dagger\|_{H^\dagger})\|\nabla E_h\delta_h\|_{0,\Omega}. \tag{4.18}$$

Finally, we will bound the term T_2^c in (4.16), as follow: we use the bilinearity of form $\mathcal{A}^{\mathcal{D}}(\cdot,\cdot)$, add and subtract adequate terms, and we use the fact that $\mathcal{A}_h^{\mathcal{D}}(\widetilde{u}_h^\dagger,\phi_I)=\mathcal{B}_h^\dagger(f^\dagger,\phi_I)$ and $\mathcal{A}^{\mathcal{D}}(\widetilde{u}^\dagger,\phi)=\mathcal{B}^\dagger(f^\dagger,\phi)$, to get

$$\begin{aligned}T_2^c &:= \mathcal{A}^{\mathcal{D}}(\widetilde{u}_h^\dagger-\widetilde{u}^\dagger,\phi_I)=\mathcal{A}^{\mathcal{D}}(\widetilde{u}_h^\dagger,\phi_I)-\mathcal{A}^{\mathcal{D}}(\widetilde{u}^\dagger,\phi_I)\\ &=(\mathcal{A}^{\mathcal{D}}(\widetilde{u}_h^\dagger,\phi_I)-\mathcal{A}_h^{\mathcal{D}}(\widetilde{u}_h^\dagger,\phi_I))+(\mathcal{B}_h^\dagger(f^\dagger,\phi_I)-\mathcal{B}^\dagger(f^\dagger,\phi_I))+\mathcal{B}^\dagger(f^\dagger,\phi_I-\phi)+\mathcal{A}^{\mathcal{D}}(\widetilde{u}^\dagger,\phi-\phi_I).\end{aligned} \tag{4.19}$$

Next, from (4.17), continuity of functional $\mathcal{B}^\dagger(\cdot,\cdot)$ and Proposition 4.1, we have

$$\mathcal{A}^{\mathcal{D}}(\widetilde{u}^\dagger,\phi-\phi_I)+\mathcal{B}^\dagger(f^\dagger,\phi_I-\phi)\le Ch^{2s}(\|\widetilde{u}^\dagger\|_{2+s,\Omega}+\|f^\dagger\|_{H^\dagger})\|\nabla E_h\delta_h\|_{0,\Omega}. \tag{4.20}$$

By using the definition of the bilinear forms $\mathcal{B}^\dagger(\cdot,\cdot)$ and $\mathcal{B}_h^\dagger(\cdot,\cdot)$, approximation properties of the projector Π_K^2, the Hölder and triangle inequalities together with Proposition 4.1, we have

$$\mathcal{B}_h^\dagger(f^\dagger,\phi_I)-\mathcal{B}^\dagger(f^\dagger,\phi_I)\le Ch^{2s}\|f^\dagger\|_{H^\dagger}\|\nabla E_h\delta_h\|_{0,\Omega}. \tag{4.21}$$

The last term in (4.19) is bounded as follow: let $\widetilde{u}_\pi^\dagger,\phi_\pi$ be the approximations of $\widetilde{u}^\dagger$ and ϕ in $\mathbb{P}_2(\mathfrak{T}_h)$, such that Proposition 4.2 hold true. Then, adding and subtracting these terms and by using the consistency of bilinear form $\mathcal{A}_h^{\mathcal{D}}(\cdot,\cdot)$ (cf. Proposition 3.2), we have:

$$\begin{aligned}\mathcal{A}^{\mathcal{D}}(\widetilde{u}_h^\dagger,\phi_I)-\mathcal{A}_h^{\mathcal{D}}(\widetilde{u}_h^\dagger,\phi_I)&=\sum_{K\in\mathfrak{T}_h}[\mathcal{A}_K^{\mathcal{D}}(\widetilde{u}_h^\dagger-\widetilde{u}_\pi^\dagger,\phi_I-\phi_\pi)-\mathcal{A}_{h,K}^{\mathcal{D}}(\widetilde{u}_h^\dagger-\widetilde{u}_\pi^\dagger,\phi_I-\phi_\pi)]\\ &\le Ch^{2s}(\|\widetilde{u}^\dagger\|_{2+s,\Omega}+\|f^\dagger\|_{H^\dagger})\|\nabla E_h\delta_h\|_{0,\Omega},\end{aligned} \tag{4.22}$$

where we have used the continuity of bilinear forms $\mathcal{A}_{h,K}^{\mathcal{D}}(\cdot,\cdot)$, $\mathcal{A}_K^{\mathcal{D}}(\cdot,\cdot)$ together with Propositions 4.2 and 4.1, Theorem 4.1 and estimate (4.13). Thus, from (4.20)–(4.22), we obtain

$$T_2^c\le Ch^{2s}(\|\widetilde{u}^\dagger\|_{2+s,\Omega}+\|f^\dagger\|_{H^\dagger})\|\nabla E_h\delta_h\|_{0,\Omega}. \tag{4.23}$$

Then, inserting the estimates (4.17), (4.18) and (4.23) in (4.16), we have that

$$T_2\le Ch^{2s}(\|\widetilde{u}^\dagger\|_{2+s,\Omega}+\|f^\dagger\|_{H^\dagger})\|\nabla E_h\delta_h\|_{0,\Omega}. \tag{4.24}$$

Therefore, from (4.14), (4.15) and (4.24), we get

$$\|\nabla E_h\delta_h\|_{0,\Omega}\le Ch^{2s}(\|\widetilde{u}^\dagger\|_{2+s,\Omega}+\|f^\dagger\|_{H^\dagger}). \tag{4.25}$$

Thus, the H^1 estimate in (4.10) follows from (4.11) and (4.25).

On the other hand, the L^2 estimate in (4.10) follows from the triangle inequality, Proposition 4.1, first asset of Lemma 4.1 and Theorem 4.1. In fact,

$$\begin{aligned}\|\widetilde{u}^\dagger-\widetilde{u}_h^\dagger\|_{0,\Omega}&\le\|\widetilde{u}^\dagger-\widetilde{u}_I^\dagger\|_{0,\Omega}+\|\delta_h-E_h\delta_h\|_{0,\Omega}+\|E_h\delta_h\|_{0,\Omega}\\ &\le Ch^{2+s}\|\widetilde{u}^\dagger\|_{2+s,\Omega}+Ch^2(|\widetilde{u}_h^\dagger-\widetilde{u}^\dagger|_{2,h}+|\widetilde{u}^\dagger-\widetilde{u}_I^\dagger|_{2,h})+C|E_h\delta_h|_{1,\Omega}\\ &\le Ch^{2s}(\|\widetilde{u}^\dagger\|_{2+s,\Omega}+\|f^\dagger\|_{H^\dagger}),\end{aligned}$$

where we have used norm equivalence in $\mathcal{V}$ and estimate (4.25). The proof is complete. □

5. Spectral approximation and error estimates

In this section, we will establish convergence and error estimates of the proposed nonconforming VEM discretization for the plate vibration and buckling problems. With this aim, we will prove that $\mathcal{S}_h^\dagger$ provides a correct spectral approximation of $\mathcal{S}^\dagger$ using the classical theory for compact operators (see [31]).

Next, an immediate consequence of Theorems 4.1 and 4.2 is that isolated parts of $sp(\mathcal{S}^\dagger)$ are approximated by isolated parts of $sp(\mathcal{S}_h^\dagger)$. It means that if μ is a nonzero eigenvalue of $\mathcal{S}^\dagger$ with algebraic multiplicity m, hence there exist m eigenvalues $\mu_h^{(1)},\dots,\mu_h^{(m)}$ of $\mathcal{S}_h^\dagger$ (repeated according to their respective multiplicities) that will converge to μ as h goes to zero.

In what follows, we denote by $\mathcal{E}$ the eigenspace of $\mathcal{S}^\dagger$ associated to the eigenvalue μ and by $\mathcal{E}_h$ the invariant subspace of $\mathcal{S}_h^\dagger$ spanned by the eigenspaces of $\mathcal{S}_h^\dagger$ associated to $\mu_h^{(1)},\dots,\mu_h^{(m)}$

We also recall the definition of the *gap* $\hat{\delta}$ between two closed subspaces $\mathcal{X}$ and $\mathcal{Y}$ of $H^\dagger$:

$$\hat{\delta}(\mathcal{X},\mathcal{Y}):=\max\{\delta(\mathcal{X},\mathcal{Y}),\delta(\mathcal{Y},\mathcal{X})\},$$

where

$$\delta(\mathcal{X},\mathcal{Y}) := \sup_{\mathbf{x}\in\mathcal{X}:\ \|x\|_{H^\dagger}=1} \delta(x,\mathcal{Y}), \quad \text{with } \delta(x,\mathcal{Y}) := \inf_{y\in\mathcal{Y}} \|x-y\|_{H^\dagger}.$$

We also define

$$\gamma_h := \sup_{v\in\mathcal{E}:\|v\|_{H^\dagger}=1} \|(\mathcal{S}^\dagger - \mathcal{S}_h^\dagger)v\|_{H^\dagger}.$$

The following error estimates for the approximation of eigenvalues and eigenfunctions hold true. The result can be obtained from Theorems 7.1 and 7.3 from [31].

Theorem 5.1. *There exists a strictly positive constant C such that*

$$\hat{\delta}(\mathcal{E},\mathcal{E}_h) \le C\gamma_h,$$
$$\left|\mu - \mu_h^{(j)}\right| \le C\gamma_h \qquad \forall j = 1,\dots,m.$$

Moreover, employing the additional regularity of the eigenfunctions, we immediately obtain the following bound.

Theorem 5.2. *There exist $s > 1/2$ and $C > 0$ independent of h such that*

$$\|(\mathcal{S}^\dagger - \mathcal{S}_h^\dagger)v\|_{H^\dagger} \le Ch^{2s}\|v\|_{H^\dagger} \qquad \forall v \in \mathcal{E}, \tag{5.1}$$

and as a consequence,

$$\gamma_h \le Ch^{2s}. \tag{5.2}$$

Proof. The inequality (5.1) is obtained repeating the proof of Theorem 4.2. Estimate (5.2) follows from the definition of γ_h and (5.1). □

Remark 5.1. In the above convergence analysis, we have considered C^0-nonconforming VEM methods to propose discrete schemes and unified analysis of source problems associated with both **VEP** and **BEP**. Moreover, one can employ fully nonconforming Morley type VEM [20] for approximating both eigenvalue problems. On the one hand, to analyze the **VEP**, we can define a continuous source operator from $L^2(\Omega)$ and the corresponding discrete source operator on $L^2(\Omega)$, and the convergence of the operator directly follows from Babuška–Osborn spectral theory [31] of a compact operator. On the other hand, the convergence analysis of **BEP** is not straightforward, since we need an additional regularity of the source function to define a suitable source operator. Thus, further research is needed for the convergence analysis in this case.

6. Numerical results

In this section, we would like to discuss some numerical experiments to confirm the theoretical expectation for rate of convergences of the eigenvalues. The work-ability of the proposed schemes are justified with nonconvex and even more general type of polygonal domain with circular holes inside the domain. The domain is discretized with different type of polygonal elements such as nonconvex, voronoi, square, and uniform polygonal elements as shown in Fig. 1. Further, by using standard basis of virtual space, Problem 2 leads to a generalized matrix eigenvalue problem (for **BEP** or **VEP**) of the form

$$\mathbf{A}\boldsymbol{u} = \lambda_h \mathbf{B}\boldsymbol{u},$$

where $\boldsymbol{u}$ is the vector of components of the corresponding eigenfunction in the chosen basis. Matrix $\mathbf{A}$ is symmetric and positive definite and $\mathbf{B}$ is symmetric and semipositive definite. Therefore, we have solved (by using MATLAB command `eigs`) the following equivalent problem

$$\mathbf{B}\boldsymbol{u} = \frac{1}{\lambda_h}\mathbf{A}\boldsymbol{u}.$$

Eventually, to compare the approximated eigenvalues of **BEP**, we introduce the following buckling coefficient [7],

$$\widetilde{\lambda}_h^{(j)} := \frac{\lambda_h^{(j)} L^2}{\pi^2},$$

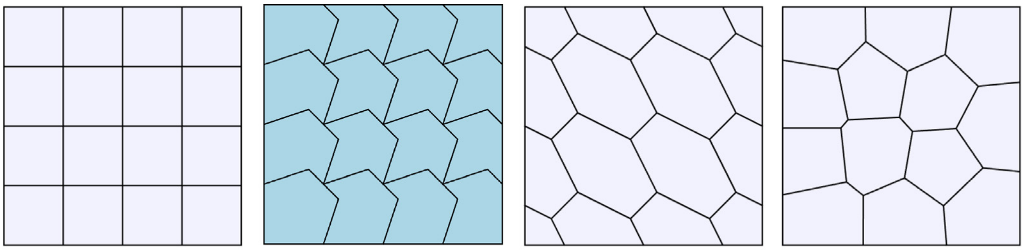

(a) (b) (c) (d)

Fig. 1. Domain discretized with different meshes: (a) Square, (b) nonconvex mesh, (c) regular polygon and (d) Voronoi mesh.

where L is the side-length of the plate. The eigenvalues of **VEP** are directly compared with the published results in Refs. [6,7]. Moreover, to investigate the buckling coefficients and corresponding buckling modes of **BEP** for different choice of stress tensors $\boldsymbol{\eta}$ numerically, such as

$$\boldsymbol{\eta}_1 := \begin{pmatrix} 1 & 0 \\ 0 & 1 \end{pmatrix}, \qquad \boldsymbol{\eta}_2 := \begin{pmatrix} 1 & 0 \\ 0 & 0 \end{pmatrix}, \qquad \boldsymbol{\eta}_3 := \begin{pmatrix} 0 & 1 \\ 1 & 0 \end{pmatrix}, \tag{6.1}$$

we will recast the bilinear form as $\mathcal{B}^{\nabla}(u, v) := (\boldsymbol{\eta}\nabla u, \nabla v)_{0,\Omega}$ for all $u, v \in \mathcal{V}$, in order to cover more general scenarios than uniformly compressed plates (covered by our the theory). We will also consider circular domains and mixed boundary conditions (cf. Remark 2.1) in the numerical examples. For better representation of the article, we denote the meshes with square, nonconvex, regular polygon, and voronoi by $\mathfrak{T}_h^1$, $\mathfrak{T}_h^2$, $\mathfrak{T}_h^3$, and $\mathfrak{T}_h^4$ respectively. The refinement parameter N denotes the number of elements on each edge of the plate.

6.1. Experiment 1: Convex domain with clamped and mixed boundary conditions

In this experiment, we have considered the computational domain $\Omega = (0, 1) \times (0, 1)$, and carried out vibration and buckling problems with clamped and mixed boundary conditions. In first case, we consider $\boldsymbol{\eta}_1$ as stress tensor for the buckling problem with clamped boundary condition. In second case, we have considered

$$\boldsymbol{\eta} := \begin{pmatrix} 1 - \frac{\alpha y}{L} & 0 \\ 0 & 0 \end{pmatrix} \tag{6.2}$$

as stress tensor, and different boundary conditions on different edges, e.g., simply supported (S.S.) boundary condition is imposed on two edges which are parallel to vertical axis, and free boundary condition is imposed on two edges which are parallel to horizontal axis. For future references, we call this type configuration of boundary conditions as *mixed boundary conditions* where different boundary conditions are applied on different parts of the boundary. We have carried out the numerical test for vibration problem with analogous boundary conditions. In Tables 1, and 3, we display the numerical results for **VEP** with clamped and mixed boundary conditions, whereas in Tables 2, and 4, we post the results for **BEP** with clamped and mixed boundary conditions. The posted values are compared with the papers [6,7], and the numerical results matches with the theoretical prediction. We have displayed the eigenfunctions corresponding to the first and second eigenvalues of **VEP** and **BEP** with clamped boundary condition in Figs. 2, and 3 respectively. We have chosen $\alpha = 0, 2/3, 1, 2$ for the plane stress tensor to compute buckling modes of **BEP**. In Figs. 4, and 5, we have posted the eigenfunctions for **VEP**, and **BEP** respectively.

In addition to the above test, we would like to discuss a comparison of our scheme with the C^1-conforming method as proposed in [6]. We have assessed **VEP** on square domain $\overline{\Omega} = [0, 1] \times [0, 1]$ with simply supported boundary condition on $\partial\Omega$. The computed eigenvalues in both methods are posted in Table 5, and associated errors are measured with the exact solutions. Further, we denote the exact eigenvalues by λ^i, and approximated eigenvalues in C^1-conforming scheme and C^0-nonconforming scheme are denoted by $\lambda_h^{i,c}$, and $\lambda_h^{i,nc}$, respectively, where $i \in \{1, 2, 3, 4\}$. We have carried out the test with stabilized biharmonic matrix and with only polynomial part of the mass matrix. From the proposed results, we deduce that C^0-nonconforming scheme shows slightly better results than the C^1-conforming scheme for the same values of mesh-size h. However, we have employed more information or DoFs (degrees of freedom) in C^0-nonconforming space than C^1-conforming case.

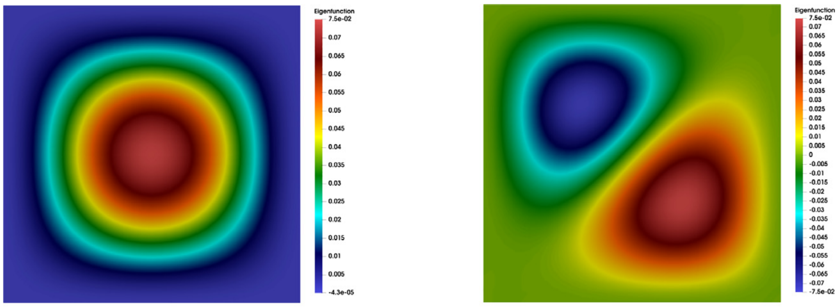

(a) (b)

Fig. 2. Experiment 1: Eigenfunctions of **VEP** with clamped boundary condition on convex plate associated with lowest eigenvalues.

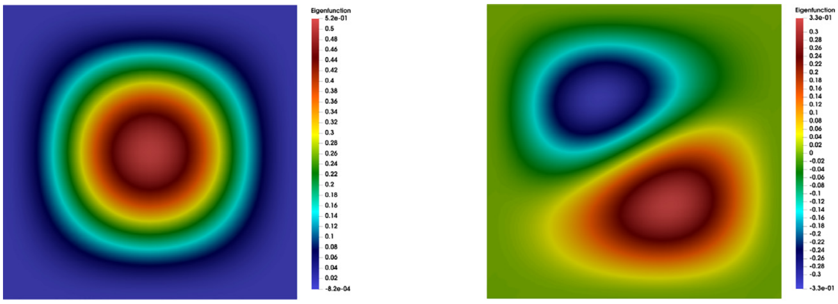

(a) (b)

Fig. 3. Experiment 1: Buckling modes of **BEP** with clamped boundary condition associated with lowest buckling coefficients.

Table 1
Experiment 1: Lowest eigenvalues of **VEP** on convex plate with clamped boundary condition.

	Mesh	$N=32$	$N=64$	$N=128$	Order	Extrapolated	[2]
λ_h^1		1211.4441	1272.7503	1289.2972	1.89	1295.4071	1294.9369
λ_h^2	$\mathfrak{T}_h^1$	4780.4382	5218.9363	5343.5380	1.82	5392.4860	5386.6675
λ_h^3		4780.4382	5218.9363	5343.5380	1.82	5392.4860	5386.6675
λ_h^4		10 213.8381	11 284.8991	11 600.3079	1.76	11 733.0268	11 710.9076
λ_h^1		1208.8418	1271.9642	1288.2973	1.95	1294.0034	1294.9369
λ_h^2	$\mathfrak{T}_h^2$	4753.9031	5210.6824	5339.5380	1.83	5389.6992	5386.6675
λ_h^3		4783.1465	5219.5120	5339.5380	1.86	5385.2997	5386.6675
λ_h^4		10 142.2229	11 261.8057	11 580.3079	1.81	11 707.9368	11 710.9076
λ_h^1		1178.5009	1262.1061	1284.5102	1.90	1292.7086	1294.9369
λ_h^2	$\mathfrak{T}_h^3$	4588.1160	5151.6678	5315.3801	1.78	5382.9047	5386.6675
λ_h^3		4610.4710	5159.0443	5320.3791	1.77	5386.9625	5386.6675
λ_h^4		9519.2784	11 030.3153	11 500.1013	1.69	11 710.0237	11 710.9076
λ_h^1		1192.1119	1266.5486	1287.5261	1.83	1295.7067	1294.9369
λ_h^2	$\mathfrak{T}_h^4$	4665.0228	5181.7519	5333.3904	1.77	5396.2056	5386.6675
λ_h^3		4697.4876	5181.7324	5333.8086	1.75	5395.3747	5386.6675
λ_h^4		9725.1085	11 108.3919	11 550.9003	1.64	11 760.9372	11 710.9076

Table 2
Experiment 1: Lowest non dimensional buckling coefficients of **BEP** with clamped boundary condition.

	Mesh	$N = 32$	$N = 64$	$N = 128$	Order	Extrapolated	[7]
$\widehat{\lambda}_h^1$		5.1985	5.2752	5.2962	1.86	5.3043	5.3038
$\widehat{\lambda}_h^2$	$\mathfrak{T}_h^4$	8.9752	9.2444	9.3111	2.01	9.3332	9.3350
$\widehat{\lambda}_h^3$		8.9924	9.2456	9.3113	1.95	9.3342	9.3347
$\widehat{\lambda}_h^4$		12.3110	12.8097	12.9433	1.90	12.9922	12.9907
$\widehat{\lambda}_h^1$		5.2543	5.2914	5.3006	2.01	5.3036	5.3038
$\widehat{\lambda}_h^2$	$\mathfrak{T}_h^1$	9.0948	9.2769	9.3199	2.08	9.3333	9.3350
$\widehat{\lambda}_h^3$		9.0948	9.2769	9.3199	2.08	9.3333	9.3347
$\widehat{\lambda}_h^4$		12.6589	12.9115	12.9708	2.09	12.9891	12.9907
$\widehat{\lambda}_h^1$		5.2483	5.2898	5.3012	1.87	5.3054	5.3038
$\widehat{\lambda}_h^2$	$\mathfrak{T}_h^2$	9.0853	9.2746	9.3189	2.10	9.3323	9.3350
$\widehat{\lambda}_h^3$		9.0872	9.2750	9.3189	2.10	9.3323	9.3347
$\widehat{\lambda}_h^4$		12.6158	12.9005	12.9608	2.24	12.9769	12.9907
$\widehat{\lambda}_h^1$		5.1762	5.2691	5.2932	1.95	5.3016	5.3038
$\widehat{\lambda}_h^2$	$\mathfrak{T}_h^3$	8.8966	9.2215	9.2931	2.18	9.3134	9.3350
$\widehat{\lambda}_h^3$		8.9291	9.2289	9.2932	2.22	9.3108	9.3347
$\widehat{\lambda}_h^4$		12.1755	12.7730	12.9191	2.03	12.9666	12.9907

Table 3
Experiment 1: Lowest eigenvalues of **VEP** on convex plate with mixed boundary condition.

	Mesh	$N = 32$	$N = 64$	$N = 128$	Order	Extrapolated
λ_h^1		93.2060	94.0167	94.2270	1.95	94.3001
λ_h^2	$\mathfrak{T}_h^1$	270.0535	271.4648	271.8102	2.03	271.9223
λ_h^3		1362.1197	1376.9642	1380.6514	2.01	1381.8681
λ_h^4		1462.1930	1513.1605	1525.8210	2.01	1529.9980
λ_h^1		93.28864	94.0379	94.2273	1.98	94.2919
λ_h^2	$\mathfrak{T}_h^2$	269.9777	271.4466	271.8191	1.98	271.9455
λ_h^3		1359.4812	1376.2944	1380.6247	1.96	1382.1167
λ_h^4		1466.2685	1514.2933	1526.8184	1.94	1531.2271
λ_h^1		93.1347	93.9897	94.2100	1.96	94.2859
λ_h^2	$\mathfrak{T}_h^3$	267.6528	270.8241	271.7123	2.01	271.8715
λ_h^3		1336.5547	1370.1006	1380.1098	2.01	1380.6005
λ_h^4		1456.8160	1511.1680	1521.7532	1.96	1529.9811
λ_h^1		91.7032	93.3979	93.9815	1.54	94.2864
λ_h^2	$\mathfrak{T}_h^4$	257.7756	267.2632	270.2094	1.69	271.5214
λ_h^3		1300.4466	1356.7263	1373.3834	1.76	1380.3328
λ_h^4		1436.4495	1502.6499	1521.8618	1.79	1529.6541

6.2. Experiment 2: Circular domain with clamped boundary condition

In this example, we have studied **VEP** and **BEP** on a circular disk with clamped boundary condition. The computational domain is considered as $\Omega := \{(x, y) \in \mathbb{R}^2 : (x)^2 + (y)^2 < 0.5\}$. We approximate the eigenvalues for **BEP** with the stress tensor $\boldsymbol{\eta}_1$, and the approximated eigenvalues are posted in Table 7. In Table 6, we have posted the results for **VEP**. In Figs. 6, and 7, we have posted the eigenfunctions for **VEB** and **BEP** respectively. To compute buckling coefficients, we have set $L = 1$. In this numerical test, a variational crime arises by approximating the curved domain with a polygonal one. However, we observe from the results reported in Tables 7 and 6 that the order of convergence for the two methods is quadratic.

Table 4
Experiment 1: Lowest non dimensional buckling coefficients of **BEP** with mixed boundary condition with $\alpha = 2/3$.

	Mesh	$N = 32$	$N = 64$	$N = 128$	Order	Extrapolated	[7]
$\widehat{\lambda}_h^1$		1.3872	1.3899	1.3906	1.97	1.3908	1.4496
$\widehat{\lambda}_h^2$	$\mathfrak{T}_h^1$	4.6914	4.7051	4.7084	2.08	4.7094	
$\widehat{\lambda}_h^3$		5.1285	5.1620	5.1706	1.97	5.1735	
$\widehat{\lambda}_h^4$		10.1016	10.1570	10.1715	1.92	10.1767	
$\widehat{\lambda}_h^1$		1.3873	1.3899	1.3905	1.99	1.3908	1.4496
$\widehat{\lambda}_h^2$	$\mathfrak{T}_h^2$	4.6863	4.7038	4.7082	1.97	4.7098	
$\widehat{\lambda}_h^3$		5.1292	5.1621	5.1708	1.97	5.1735	
$\widehat{\lambda}_h^4$		10.0920	10.1543	10.1704	1.96	10.1760	
$\widehat{\lambda}_h^4$		1.3849	1.3892	1.3904	1.90	1.3908	1.4496
$\widehat{\lambda}_h^4$	$\mathfrak{T}_h^3$	4.6427	4.6920	4.7044	1.99	4.7085	
$\widehat{\lambda}_h^4$		5.0919	5.1513	5.1661	2.01	5.1710	
$\widehat{\lambda}_h^4$		9.9395	10.1129	10.1592	1.90	10.1762	
$\widehat{\lambda}_h^4$		1.3690	1.3844	1.3885	1.90	1.3900	1.4496
$\widehat{\lambda}_h^4$	$\mathfrak{T}_h^4$	4.4925	4.6330	4.6809	1.55	4.7058	
$\widehat{\lambda}_h^4$		5.0371	5.1495	5.1663	2.75	5.1691	
$\widehat{\lambda}_h^4$		9.7098	10.0076	10.1123	1.51	10.1688	

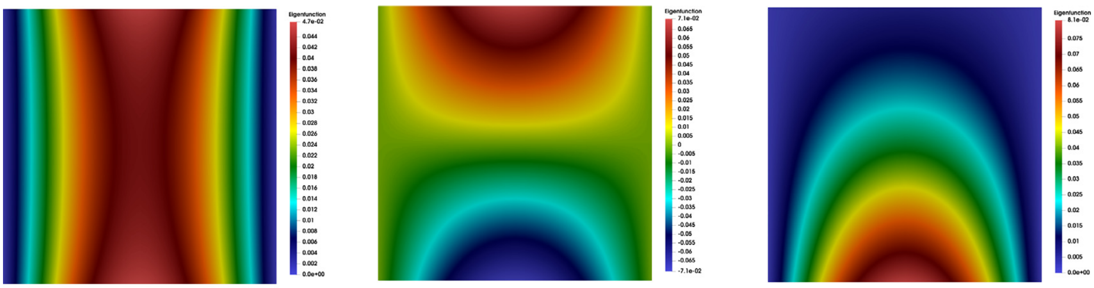

(a) (b) (c)

Fig. 4. Experiment 1: First and second eigenfunctions of **VEP** on convex plate with mixed boundary condition; right most panel shows the first buckling mode of **BEP** with mixed boundary condition for $\alpha = 2$.

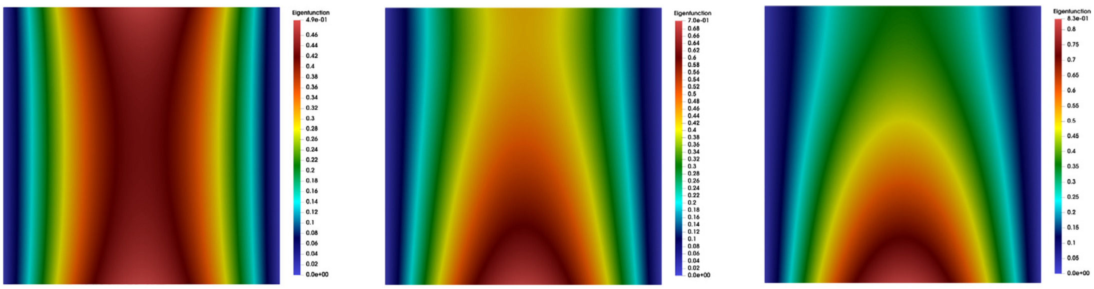

(a) (b) (c)

Fig. 5. Experiment 1: First buckling modes of **BEP** with mixed boundary condition for different values of α, such as, $\alpha = 0, 2/3, 1$ respectively.

Table 5
Experiment 1: Comparison between approximations of lowest eigenvalues of **VEP** on unit square plate with simply supported boundary conditions computed with C^0-nonconforming method, and C^1-conforming method.

	Mesh	λ^1	$\lambda_h^{1,c}$	$\lvert\lambda^1-\lambda_h^{1,c}\rvert$	$\lambda_h^{1,nc}$	$\lvert\lambda 1-\lambda_h^{1,nc}\rvert$
$N=16$		389.636364	391.240119	1.603755	388.451634	1.184730
$N=32$	$\mathfrak{T}_h^1$	389.636364	390.018435	0.382071	389.335995	0.300368
$N=64$		389.636364	389.730660	0.094296	389.561007	0.075364
$N=128$		389.636364	389.659857	0.023493	389.617497	0.018867
		λ^2	$\lambda_h^{2,c}$	$\lvert\lambda_2-\lambda_h^{2,c}\rvert$	$\lambda_h^{2,nc}$	$\lvert\lambda_2-\lambda_h^{2,nc}\rvert$
$N=16$		2435.227275	2419.499820	15.727455	2433.991981	1.235294
$N=32$	$\mathfrak{T}_h^1$	2435.227275	2430.218421	5.008854	2434.803281	0.423994
$N=64$		2435.227275	2433.902424	1.324851	2435.114019	0.113256
$N=128$		2435.227275	2434.891424	0.335851	2435.198496	0.028779
		λ^3	$\lambda_h^{3,c}$	$\lvert\lambda_3-\lambda_h^{3,c}\rvert$	$\lambda_h^{3,nc}$	$\lvert\lambda_3-\lambda_h^{3,nc}\rvert$
$N=16$		2435.227275	2419.499827	15.727448	2433.991981	1.235294
$N=32$	$\mathfrak{T}_h^1$	2435.227275	2430.218421	5.008854	2434.803281	0.423994
$N=64$		2435.227275	2433.902424	1.324851	2435.114019	0.113256
$N=128$		2435.227275	2434.891424	0.335850	2435.198496	0.028779
		λ^4	$\lambda_h^{4,c}$	$\lvert\lambda_4-\lambda_h^{4,c}\rvert$	$\lambda_h^{4,nc}$	$\lvert\lambda_4-\lambda_h^{4,nc}\rvert$
$N=16$		6234.181826	6354.018452	119.836626	6162.519753	71.662073
$N=32$	$\mathfrak{T}_h^1$	6234.181826	6259.845048	25.663222	6215.226149	18.955676
$N=64$		6234.181826	6240.295102	6.113276	6229.375927	4.805898
$N=128$		6234.181826	6235.690579	1.508753	6232.976122	1.205703

Table 6
Experiment 2: Eigenvalues of **VEP** on circular plate with clamped boundary condition.

	Mesh	$N=64$	$N=128$	$N=256$	Order	Extrapolated
λ_h^1		1643.5555	1663.1962	1668.3615	1.96	1669.9927
λ_h^2	$\mathfrak{T}_h^4$	7004.5797	7174.6345	7219.8921	1.94	7234.5249
λ_h^3		7019.5149	7177.2025	7219.4048	1.93	7233.2205
λ_h^4		18 549.5953	19 225.9687	194 096.1017	1.91	19 470.8582

Table 7
Experiment 2: Eigenvalues of **BEP** on circular disk with clamped boundary condition.

	Mesh	$N=64$	$N=128$	$N=256$	Order	Extrapolated	[7]
$\widehat{\lambda}_h^1$		5.9355	5.9468	5.9498	1.95	5.9507	5.9506
$\widehat{\lambda}_h^2$	$\mathfrak{T}_h^4$	10.6156	10.6711	10.6853	2.00	10.6896	10.6895
$\widehat{\lambda}_h^3$		10.6266	10.6729	10.6852	1.95	10.6891	10.6891
$\widehat{\lambda}_h^4$		16.3145	16.4518	16.4874	1.98	16.4984	16.4983

6.3. Experiment 3: Non simply connected domain with clamped-free, and S.S.-free boundary conditions

In this experiment, we have considered a complex non simply connected domain $\Omega := (0,1)\times(0,1)\backslash[1/4,3/4]\times[1/4,3/4]$ which is discretized with voronoi mesh. We have investigated the characteristic of the plate for **VEP**, and **BEP** with different boundary conditions. Further, we have experienced with two non-identical stress tensors which are applied on the plate for **BEP**, e.g., (1) forces are applied from all outside boundary of the plate ($\boldsymbol{\eta}_1$) and (2) forces are applied on the outside boundary along the tangential direction ($\boldsymbol{\eta}_3$) (for further detail, please see [7, Figure 3]). We have used the notations such as "clamped-free", or "S.S.-free" to signify that in the corresponding experiments, we have employed clamped or S.S. boundary condition on outside boundary of the plate and free boundary condition on inside boundary of the plate. In Table 8, we have posted computed eigenvalues for **VEP** with clamped-free and S.S.-free boundary conditions. In Table 9, we have displayed the computed buckling coefficients

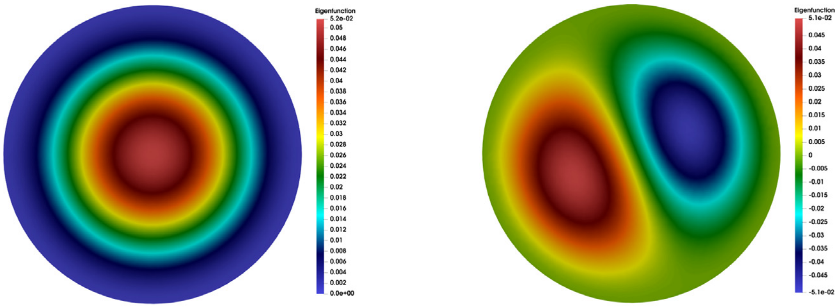

(a) (b)

Fig. 6. Experiment 2: First and second eigenfunctions of **VEP** on circular plate with clamped boundary condition.

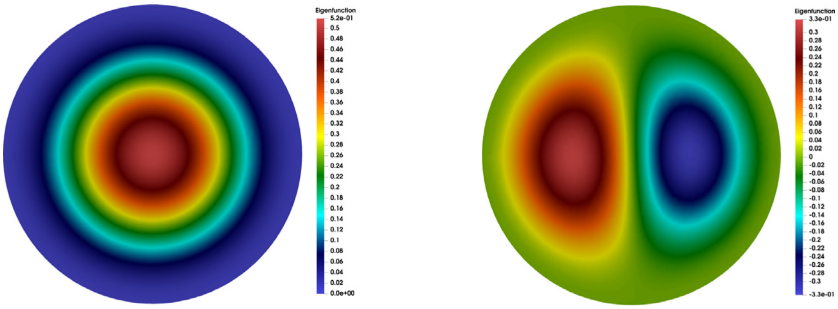

(a) (b)

Fig. 7. Experiment 2: First and second buckling modes of **BEP** on circular disk with clamped boundary condition.

Table 8
Experiment 3: First eigenvalue of **VEP** with clamped-free and S.S.-free boundary conditions.

B.C.	$\mathcal{N}_P = 256$	$\mathcal{N}_P = 1024$	$\mathcal{N}_P = 4096$
Clamped-free	3149.4529	3951.5761	4230.1721
S.S.-free	525.3662	559.5392	572.5411

Table 9
Experiment 3: First buckling coefficient of **BEP** with clamped-free and S.S.-free boundary conditions for different stress tensors $\boldsymbol{\eta}_1$, and $\boldsymbol{\eta}_3$.

B.C.	Stress tensor	$\mathcal{N}_P = 256$	$\mathcal{N}_P = 1024$	$\mathcal{N}_P = 4096$
Clamped-free	$\boldsymbol{\eta}_1$	4.7356	4.9539	5.0559
S.S.-free	$\boldsymbol{\eta}_1$	1.0080	1.0575	1.0771
Clamped-free	$\boldsymbol{\eta}_3$	13.7099	19.0897	22.5696
S.S.-free	$\boldsymbol{\eta}_3$	6.5091	8.3972	9.3331

for **BEP** with clamped-free and S.S.-free boundary conditions. In Fig. 8, we have displayed the first eigenfunctions of **VEP** corresponding to clamped-free and S.S.-free boundary conditions. In Fig. 9, we have posted first buckling modes of **BEP** corresponding to clamped-free boundary condition and for different stress tensors $\boldsymbol{\eta}_1$, and $\boldsymbol{\eta}_3$. In Fig. 10, we have shown first buckling modes with S.S.-free boundary conditions for different stress tensors such as $\boldsymbol{\eta}_1$, and $\boldsymbol{\eta}_3$. The refinement parameter $\mathcal{N}_P$ denotes the number of elements contained in the plate.

6.4. Experiment 4: Circular domain with multiple holes

In this experiment, we have carried out a numerical test on a circular plate with multiples holes where clamped and S.S. boundary conditions are applied on outside boundary and free boundary condition is imposed on internal

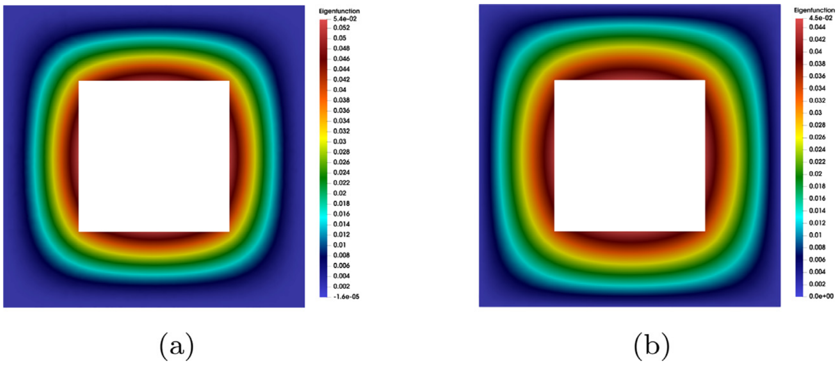

Fig. 8. Experiment 3: Left panel displays first eigenfunction of **VEP** with clamped-free boundary condition and right panel displays first eigenfunction of **VEP** with S.S.-free boundary conditions.

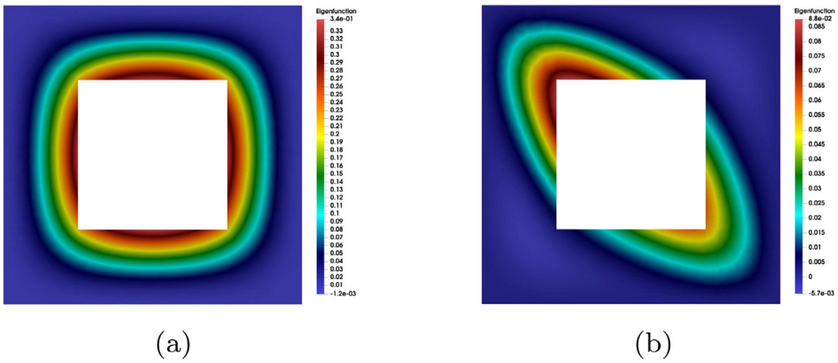

Fig. 9. Experiment 3: Left panel displays the first buckling mode of **BEP** with stress tensor $\boldsymbol{\eta}_1$, and with clamped-free boundary condition; right panel shows the first buckling mode of **BEP** with stress tensor $\boldsymbol{\eta}_3$ and with clamped-free boundary condition.

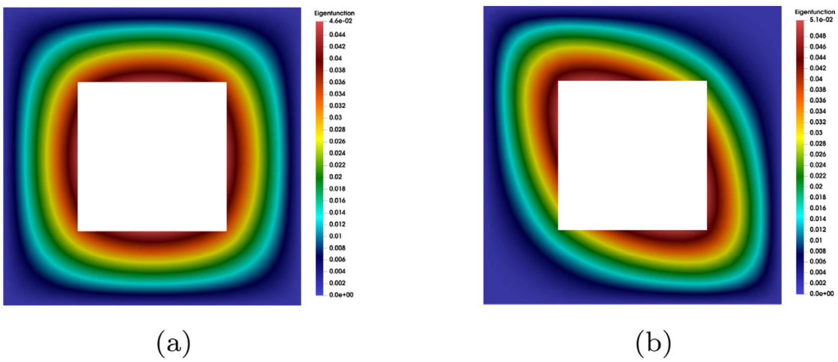

Fig. 10. Experiment 3: Left panel shows the first buckling mode of **BEP** with S.S.-free boundary condition for stress tensor $\boldsymbol{\eta}_1$; right panel displays the first buckling mode of **BEP** with S.S.-free boundary condition and with stress tensor $\boldsymbol{\eta}_3$.

boundary. More precisely, we have considered $\Omega := \Omega_C \backslash \big(\Omega_1 \cup \cdots \cup \Omega_4\big)$, where $\Omega_C := \{(x, y) \in \mathbb{R}^2 : x^2 + y^2 < 1\}$ and

$$\Omega_1 := \{(x, y) \in \mathbb{R}^2 : (x - 0.4)^2 + (y - 0.4)^2 \leq 0.04\};$$
$$\Omega_2 := \{(x, y) \in \mathbb{R}^2 : (x + 0.4)^2 + (y - 0.4)^2 \leq 0.04\};$$
$$\Omega_3 := \{(x, y) \in \mathbb{R}^2 : (x + 0.4)^2 + (y + 0.4)^2 \leq 0.04\};$$
$$\Omega_4 := \{(x, y) \in \mathbb{R}^2 : (x - 0.4)^2 + (y + 0.4)^2 \leq 0.04\}.$$

Table 10
Experiment 4: First eigenvalue of **VEP** with clamped-free boundary condition; First buckling coefficient of **BEP** with clamped-free boundary condition for stress tensor $\boldsymbol{\eta}_1$.

B.C.	Model problem	$\mathcal{N}_P = 1024$	$\mathcal{N}_P = 2048$	$\mathcal{N}_P = 4096$
Clamped-free	**VEP**	68.5525	70.8851	72.2133
Clamped-free	**BEP**	2.6980	2.7353	2.7559

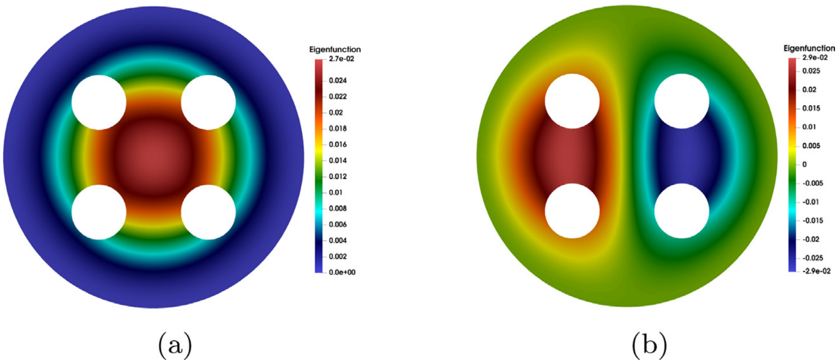

Fig. 11. Experiment 4: Eigenfunctions of **VEP** on circular plate consists of multiples holes with clamped-free boundary condition.

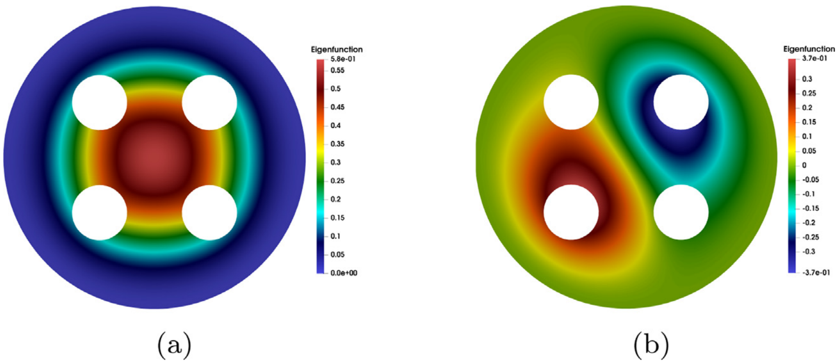

Fig. 12. Experiment 4: Buckling modes of **BEP** on circular disk consists of multiple holes with clamped-free boundary condition.

We have considered stress tensor as $\boldsymbol{\eta}_1$ for **BEP**. Numerical solution of eigenfunctions corresponding to **VEP** and **BEP** are posted in Figs. 11, and 12, respectively. Eigenvalues corresponding to **VEP** and **BEP** are posted in Table 10. To compute buckling coefficients, we have set $L = 2$.

7. Conclusion

We considered C^0-nonconforming VEM approximation of vibration and buckling eigenvalue problems. To characterize and analyze the spectrum of discrete problems, we introduced source problems connected with the considered model problems. Further, we introduced enriching operator to analysis and derive convergence theory over more general nonconvex domain. By exploiting enriching operator, we proved the convergence of the solution operator and concluded the convergence estimates of spectrum by directly applying *Babuška–Osborn* theory. Even though the theory is developed by considering clamped boundary condition of the model problem, the adjoined remark covered more general model problems including mixed boundary conditions. An extensive numerical experiments are performed to verify the theory. A numerical approximation of transmission eigenvalue problems by using nonconforming VEM would be a further field of interest.

Declaration of competing interest

The authors declare that they have no known competing financial interests or personal relationships that could have appeared to influence the work reported in this paper.

Data availability

Data will be made available on request.

Acknowledgments

The first author was partially supported by the National Agency for Research and Development, ANID-Chile through FONDECYT Postdoctorado project 3200242. The second author was partially supported by DICREA, Chile through project 2120173 GI/C Universidad del Bío-Bío, by the National Agency for Research and Development, ANID-Chile through FONDECYT project 1220881, and by project Centro de Modelamiento Matemático (CMM), Chile FB210005, BASAL funds for centers of excellence and by project ECOS-ANID, Chile ECOS200038-C20E05.

References

[1] C. Carstensen, D. Gallistl, Guaranteed lower eigenvalue bounds for the biharmonic equation, Numer. Math. 126 (1) (2014) 33–51.
[2] D. Mora, R. Rodríguez, A piecewise linear finite element method for the buckling and the vibration problems of thin plates, Math. Comp. 78 (268) (2009) 1891–1917.
[3] R. Rannacher, Nonconforming finite element methods for eigenvalue problems in linear plate theory, Numer. Math. 33 (1979) 23–42.
[4] K. Ishihara, On the mixed finite element approximation for the buckling of plates, Numer. Math. 33 (2) (1979) 195–210.
[5] D. Mora, I. Velásquez, A virtual element method for the transmission eigenvalue problem, Math. Models Methods Appl. Sci. 28 (14) (2018) 2803–2831.
[6] D. Mora, G. Rivera, I. Velásquez, A virtual element method for the vibration problem of Kirchhoff plates, ESAIM Math. Model. Numer. Anal. 52 (4) (2018) 1437–1456.
[7] D. Mora, I. Velásquez, Virtual element for the buckling problem of Kirchhoff–Love plates, Comput. Methods Appl. Mech. Engrg. 360 (2020).
[8] F. Dassi, I. Velásquez, Virtual element method on polyhedral meshes for bi-harmonic eigenvalues problems, Comput. Math. Appl. 121 (2022) 85–101.
[9] L. Beirão da Veiga, F. Brezzi, L.D. Marini, A. Russo, Mixed virtual element methods for general second order elliptic problems on polygonal meshes, ESAIM Math. Model. Numer. Anal. 50 (3) (2016) 727–747.
[10] L. Beirão da Veiga, F. Brezzi, L.D. Marini, A. Russo, Virtual element method for general second-order elliptic problems on polygonal meshes, Math. Models Methods Appl. Sci. 26 (4) (2016) 729–750.
[11] A. Cangiani, P. Chatzipantelidis, G. Diwan, E.H. Georgoulis, Virtual element method for quasilinear elliptic problems, IMA J. Numer. Anal. 40 (4) (2020) 2450–2472.
[12] Y. Wang, G. Wang, A least-squares virtual element method for second-order elliptic problems, Comput. Math. Appl. 80 (8) (2020) 1873–1886.
[13] M.F. Benedetto, S. Berrone, A. Borio, S. Pieraccini, S. Scialò, Order preserving SUPG stabilization for the virtual element formulation of advection-diffusion problems, Comput. Methods Appl. Mech. Engrg. 311 (2016) 18–40.
[14] S. Berrone, A. Borio, G. Manzini, SUPG stabilization for the nonconforming virtual element method for advection–diffusion–reaction equations, Comput. Methods Appl. Mech. Engrg. 340 (2018) 500–529.
[15] D. Adak, D. Mora, S. Natarajan, Convergence analysis of virtual element method for nonlinear nonlocal dynamic plate equation, J. Sci. Comput. 91 (1) (2022) 1–37.
[16] B. Ayuso de Dios, K. Lipnikov, G. Manzini, The nonconforming virtual element method, ESAIM Math. Model. Numer. Anal. 50 (3) (2016) 879–904.
[17] J. Zhao, B. Zhang, S. Mao, S. Chen, The divergence-free nonconforming virtual element for the Stokes problem, SIAM J. Numer. Anal. 57 (6) (2019) 2730–2759.
[18] A. Cangiani, V. Gyrya, G. Manzini, The nonconforming virtual element method for the Stokes equations, SIAM J. Numer. Anal. 54 (6) (2016) 3411–3435.
[19] F. Gardini, G. Manzini, G. Vacca, The nonconforming virtual element method for eigenvalue problems, ESAIM Math. Model. Numer. Anal. 53 (3) (2019).
[20] J. Zhao, B. Zhang, S. Chen, S. Mao, The Morley-type virtual element for plate bending problems, J. Sci. Comput. 76 (1) (2018) 610–629.
[21] J. Zhao, S. Chen, B. Zhang, The nonconforming virtual element method for plate bending problems, Math. Models Methods Appl. Sci. 26 (09) (2016) 1671–1687.
[22] A. Dedner, A. Hodson, Robust nonconforming virtual element methods for general fourth-order problems with varying coefficients, IMA J. Numer. Anal. 42 (2) (2022) 1364–1399.

[23] M. Li, J. Zhao, C. Huang, S. Chen, Conforming and nonconforming VEMs for the fourth-order reaction-subdiffusion equation: a unified framework, IMA J. Numer. Anal. 10 (2021).
[24] C. Carstensen, R. Khot, A. Pani, Nonconforming virtual elements for the biharmonic equation with morley degrees of freedom on polygonal meshes, 2022, arXiv:2205.08764 [math.NA].
[25] L. Chen, X. Huang, Nonconforming virtual element method for $2m$th order partial differential equations in $\mathbb{R}^n$, Math. Comp. 89 (324) (2020) 1711–1744.
[26] F. Gardini, G. Vacca, Virtual element method for second-order elliptic eigenvalue problems, IMA J. Numer. Anal. 38 (4) (2018) 2026–2054.
[27] D. Mora, G. Rivera, R. Rodríguez, A virtual element method for the Steklov eigenvalue problem, Math. Models Methods Appl. Sci. 25 (8) (2015) 1421–1445.
[28] F. Lepe, G. Rivera, A priori error analysis for a mixed VEM discretization of the spectral problem for the Laplacian operator, Calcolo 58 (2) (2021) Paper No. 20, 30.
[29] F. Lepe, D. Mora, G. Rivera, I. Velásquez, A virtual element method for the steklov eigenvalue problem allowing small edges, J. Sci. Comput. 88 (2) (2021) Paper No. 44, 21.
[30] J. Meng, L. Mei, A mixed virtual element method for the vibration problem of clamped Kirchhoff plate, Adv. Comput. Math. 46 (5) (2020) Paper No. 68, 18.
[31] I. Babuška, J. Osborn, Eigenvalue Problems, Elsevier, North-Holland, 1991.
[32] D. Bonheure, F. Gazzola, E.M. Dos Santos, Periodic solutions and torsional instability in a nonlinear nonlocal plate equation, SIAM J. Numer. Anal. 51 (4) (2019) 3052–3091.
[33] R.A. Adams, J.J. Fournier, Sobolev Spaces, Elsevier, 2003.
[34] J. Huang, Y. Yu, A medius error analysis for nonconforming virtual element methods for Poisson and biharmonic equations, J. Comput. Appl. Math. 386 (2021).
[35] J. Zhao, S. Chen, B. Zhang, The nonconforming virtual element method for plate bending problems, Math. Models Methods Appl. Sci. 26 (9) (2016) 1671–1687.
[36] D. Mora, C. Reales, A. Silgado, A C^1-virtual element method of high order for the Brinkman equations in stream function formulation with pressure recovery, IMA J. Numer. Anal. 42 (4) (2022) 3632–3674.
[37] D. Adak, D. Mora, A. Silgado, A Morley-type virtual element approximation for a wind-driven ocean circulation model on polygonal meshes, 2022, https://www.ci2ma.udec.cl/publicaciones/prepublicaciones/.
[38] H. Blum, R. Rannacher, On the boundary value problem of the biharmonic operator on domains with angular corners, Math. Methods Appl. Sci. 2 (4) (1980) 556–581.
[39] F. Brezzi, L.D. Marini, Virtual element methods for plate bending problems, Comput. Methods Appl. Mech. Engrg. 253 (2013) 455–462.
[40] A. Cangiani, G. Manzini, O.J. Sutton, Conforming and nonconforming virtual element methods for elliptic problems, IMA J. Numer. Anal. 37 (3) (2017) 1317–1354.
[41] L. Beirão da Veiga, C. Lovadina, A. Russo, Stability analysis for the virtual element method, Math. Models Methods Appl. Sci. 27 (13) (2017) 2557–2594.
[42] S.C. Brenner, L.-Y. Sung, Virtual element methods on meshes with small edges or faces, Math. Models Methods Appl. Sci. 28 (7) (2018) 1291–1336.
[43] J. Descloux, N. Nassif, J. Rappaz, On spectral approximation. Part 2. Error estimates for the Galerkin method, RAIRO Anal. Numér. 12 (2) (1978) 113–119.
[44] J. Descloux, N. Nassif, J. Rappaz, On spectral approximation. Part 1. The problem of convergence, RAIRO Anal. Numér. 12 (2) (1978) 97–112.
[45] P.F. Antonietti, L. Beirão da Veiga, S. Scacchi, M. Verani, A C^1 virtual element method for the cahn-hilliard equation with polygonal meshes, SIAM J. Numer. Anal. 54 (1) (2016) 34–56.
[46] P.F. Antonietti, G. Manzini, M. Verani, The fully nonconforming virtual element method for biharmonic problems, Math. Models Methods Appl. Sci. 28 (02) (2018) 387–407.
[47] S.C. Brenner, L.R. Scott, The Mathematical Theory of Finite Element Methods, Springer, New York, 2008.